Food Hydrocolloids 154 (2024) 110140

Contents lists available at ScienceDirect

Food Hydrocolloids

journal homepage: www.elsevier.com/locate/foodhyd

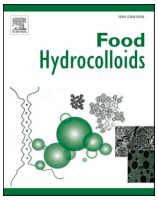

Impact of thermosonication at neutral pH on the structural characteristics of faba bean protein isolate dispersions and their physicochemical and techno-functional properties

Yinxuan Hu [a], Lirong Cheng [b,**], Elliot Paul Gilbert [c,d], Sung Je Lee [a], Zhi Yang [a,*]

[a] School of Food and Advanced Technology, Massey University, Auckland, 0632, New Zealand
[b] Riddet Institute, Massey University, Palmerston North, 4472, New Zealand
[c] Australian Centre for Neutron Scattering, ANSTO, New Illawarra Road, Lucas Heights, NSW, 2234, Australia
[d] Centre for Nutrition and Food Sciences, The University of Queensland, St. Lucia, Brisbane, QLD 4072, Australia

ARTICLE INFO

Keywords:
Thermosonication
Faba bean protein isolates
Viscoelasticity
O/W emulsions
Microstructure

ABSTRACT

The effect of thermosonication (TS) (90 °C, 10–30 min) on faba bean protein isolate (FPI) at pH 7 was investigated. The microstructural and techno-functional properties of TS-treated FPI were compared with native FPI or FPI treated with conventional prolonged heating (CH, up to 8 h) at 90 °C. TS treatment effectively converted FPI to amorphous aggregates containing predominant β-sheet secondary structures, as determined by Thioflavin T (ThT) fluorescence and circular dichroism (CD). According to sodium dodecyl sulphate-polyacrylamide gel electrophoresis (SDS-PAGE), these amorphous aggregates could be formed by disulfide bonds. Additionally, TS treatment is efficient in disrupting large protein aggregates of FPI, thus improving their solubility. Both TS and CH treatments induced formation of viscoelastic FPI hydrogels, whose gel strength depends on the type and time of treatment. Hydrogels formation is likely to arise from the entanglement and interaction of protein aggregates as revealed by small angle neutron scattering (SANS) and scanning electron microscopy (SEM). TS-treated FPI was also used to prepare O/W emulsions and whose structural and physical properties were compared with those stabilised by untreated FPI. At all oil volume fractions ($\varphi = 0.2$, 0.5, and 0.7) and FPI concentrations (1, 3, and 5 wt %), emulsions stabilised by TS-treated FPI exhibited smaller oil droplet size, greater mechanical strength and superior stability compared to those stabilised by untreated FPI. The study suggests that TS treatment is promising in improving techno-functional properties of FPI; further studies are needed to exploit TS-treated plant proteins as a novel food ingredient in food product development.

1. Introduction

Owing to its high protein content (27–36 w/w%), low allergenicity and high nutritive value, faba bean (*Vicia faba*) is one of the most popular plant foods (Augustin & Cole, 2022). It has recently attracted attention as a sustainable plant protein in the food industry (Augustin et al., 2022; Samaei et al., 2020). However, like other plant protein ingredients, faba bean protein isolate (FPI) generally exhibits poor techno-functional characteristics, such as low solubility and unfavourable emulsifying capability in comparison with animal proteins (Schwenke, 2001; Tamang et al., 2021). Therefore, various modification strategies including physical methods (e.g. ultrasonication (McCarthy, et al., 2016), heat treatment (Yang, et al., 2022), and high hydrostatic pressure (Luo, Yang, Wang, Ashokkumar, & Hemar, 2022)), chemical methods (e.g. pH shifting (Jiang, Wang, & Xiong, 2018)), and biochemical methods (e.g. enzymatic hydrolysis (Wang, Cheng, Wang, & Yang, 2022)) have been recently applied to enhance the properties of plant protein ingredients. Compared to chemical and biochemical methods, physical processing exhibits unique advantages such as the ease of operation and avoidance of the use of chemicals.

Conventional heat treatment (CH) has been extensively employed for protein modifications. Typically, the plant protein dispersions are heated above their denaturation temperature (e.g. 75–95 °C) at different pHs and/or times to allow extensive protein unfolding, denaturation, and aggregation, resulting in alterations in their techno-functional characteristics such as gelation and emulsification capabilities (Du,

* Corresponding author.
** Corresponding author.
E-mail addresses: L.cheng@massey.ac.nz (L. Cheng), Z.Yang2@massey.ac.nz (Z. Yang).

https://doi.org/10.1016/j.foodhyd.2024.110140
Received 2 February 2024; Received in revised form 24 April 2024; Accepted 24 April 2024
Available online 30 April 2024

et al., 2023; Zhu et al., 2023). For example, Jo, Huang, and Chen (2020) reported that the prolonged heat treatment (90 °C, up to 16 h) could significantly improve the gelation properties and alter the microstructural characteristics of lentil proteins. However, prolonged heating is not feasible nor sustainable for applications in food industry. CH treatment has been also used to inactivate bacteria in faba bean proteins, improve its nutritional value and sensory properties, making it safer and more acceptable for consumers (Hu, Cheng, Lee, & Yang, 2023; Karolkowski et al., 2022).

Ultrasonication (US) is another popular physical processing methods that has been employed to modify physicochemical and techno-functional properties of plant protein ingredients such as FPI (Martínez-Velasco, et al., 2018) and quinoa protein isolates (QPI) (Luo, Yang, et al., 2022). During the US treatment, high shear forces and cavitation can induce microbubbles formed in the liquid to collapse, releasing high energy locally to breakdown large protein aggregates and improve their solubility (Taha, et al., 2018; Zhang, Luo, Yang, Ashokkumar, & Hemar, 2021). However, US treatment alone is insufficient in alteration of plant protein structures for enhanced techno-functional properties (Zhong & Xiong, 2020); US has therefore been recently combined with other treatments including heat treatment (Zhong et al., 2020) and pH-shifting (Yildiz, Andrade, Engeseth, & Feng, 2017) to achieve more efficient modification of plant proteins.

Thermosonication (TS) that combines sonication and heat treatment has been demonstrated as an effective method to modify protein conformation through the combined effects of thermal energy input and ultrasound induced cavitation (Chen, Ettelaie, & Akhtar, 2019; Zhong & Xiong, 2020). Recently, Zhong and Xiong (2020) applied TS to 10 wt % mung bean protein isolates (MPI) at pH 7 at 30–70 °C for different times (5–30 min) and found that TS considerably enhanced the solubility and heat stability of MPI dispersions accompanied by alteration of protein secondary structures and conformations. In another study, Chen et al. (2019) found that TS treatment (72 °C, 10 min) could improve the efficiency of Alcalase hydrolysis of peanut protein isolates (PPI) due to the generation of fibril like protein aggregates with a high aspect ratio. Furthermore, TS has been applied as a sufficient method to inactivate microorganisms in beverages to prolong their shelf-life without damaging bioactive substances or nutrients (Guimarães, et al., 2018; Monteiro et al., 2018).

Despite TS treatment has been employed to modify plant protein dispersions, most of previous studies focused on the simple physicochemical properties such as particle size and solubility. There is scant information on protein secondary and tertiary structures, morphology, and techno-functional characteristics as affected by the TS treatment, which are imperative to elucidate process-structure-function relationship of FPI dispersions under different processing conditions. In addition, detailed comparisons of the TS treatment with conventional heating in modifications of FPI dispersions have not been conducted yet. Therefore, the present study aimed to systematically examine and compare the effect of TS and conventional heating treatment with different time (10–30 min) on protein profiles, secondary and tertiary structures, microstructural characteristics, and techno-functional properties (e.g. gelation and emulsification property) of FPI dispersions. In particular, small angle neutron scattering (SANS) was employed to reveal hierarchical structures of FPI as affected by various processing conditions in dispersion and gel states covering multiple length scales in order to gain better understanding of different nanostructure formations induced by various processing methods. This study could provide important insights on applying TS treatment to modify FPI dispersions that targets their specific requirements as texturing and emulsifying agent.

2. Materials and methods

2.1. Materials

The FPI used was acquired from NZ Protein Inc. (Auckland, New Zealand) and as stated in ingredient specifications, contains 85 wt % protein, 5.4 wt % fat, and 1 wt % carbohydrate and dietary fibre. Chemicals used in this study, such as sodium dodecyl sulphate (SDS), Fast Green, Nile Red, acetic acid, thioflavin T (ThT), low viscosity mineral oil (M 5904), HCl, and sodium azide, were of analytical grade and purchased from Sigma-Aldrich (St. Louis, MO, USA). Coomassie Brilliant Blue R-250 staining solution, β-mercaptoethanol, and 10 × Tris/Glycine/SDS running buffer were purchased from Bio-Rad (Hercules, CA, USA). All samples were prepared using Milli-Q water (Millipore, USA).

2.2. Preparation of FPI dispersions

For preparation of 10 wt% FPI stock solution, FPI powder was dispersed in 0.02 wt% sodium azide solution at 20 °C using magnetic stirring (300 rpm) for 24 h for full hydration. For pH adjustment to pH 7, aliquots of 1 M HCl was pipetted to the stock solution under stirring for 24 h, while the pH value was regularly monitored until stable. FPI dispersions at 2.5, 3, and 5 wt % were made by mixing the 10 wt% FPI solution (10 wt %) with 0.02 wt% sodium azide (pH 7) solution.

2.3. Thermosonication of FPI dispersions

FPI dispersions (10 g each, 2.5, 3, 5, and 10 wt %, pH 7) prepared as described in section 2.2 were thermosonicated for 10 min (TS-10), 20 min (TS-20), and 30 min (TS-30) (50% power amplitude, pulse durations of on-time 30 s and off-time 30 s) by a 20 kHz ultrasonicator (6 mm horn) with a dial power 950 W (JY92-IIN, Ningbo Scientz Biotechnology Co., ltd, China) in a 20 mL glass vials at 90 °C in a jacket bottle (100 mL, Shanghai Leigu Instrument Ltd, China) connected with a temperature-controlled water bath (Thermofisher, USA). To compensate for water evaporation during the TS treatment, samples were supplemented with Milli-Q water (pH 7) to the original weight. All samples were prepared in duplicate and kept at 20 °C for 24 h before characterisation. Conventional heat treatment was conducted according to Wynnychuk, Jo, Chu, and Chen (2021) with slight modifications. FPI dispersions were heated at 90 °C for 1 h (CH-1), 4 h (CH-4), and 8 h (CH-8) in an air oven (Thermofisher, USA). The control samples in this study were defined as the FPI dispersions without any treatment.

2.4. Physico-chemical characterisations of FPI dispersions

2.4.1. Sodium dodecyl sulphate–polyacrylamide gel electrophoresis (SDS-PAGE)

Reducing and non-reducing SDS-PAGE was performed according to Laemmli (1970) and our previous study (Hu, et al., 2023).

2.4.2. Determination of FPI particle size

A ZetaSizer Nano ZS (Malvern instruments, UK) was utilized to measure particle size of control and treated FPI dispersions (2.5 wt %) at 20 °C. The laser scattering angle is 173° and wavelength is 633 nm. The FPI dispersion was diluted one hundred times in Milli-Q water before measurements, using the refractive index and viscosity of dispersant (water) of 1.33 and 0.89 mPa s, respectively (Luo, Yang, et al., 2022). Triplicate measurements were performed for each sample and results are represented as z-average size.

2.4.3. Determination of FPI solubility

The solubility of FPI at 2.5 wt % after various treatments was determined following the method of Hu et al. (2023) with small modifications. A centrifuge (Thermofisher 3000, MO, USA) was used to

centrifuge the FPI dispersions at 3000×*g* for 15 min at ~20 °C and supernatant was collected. After that, soluble protein content was quantified from the supernatant using the Bradford Protein Assay Kit (Sigma-Aldrich, St. Louis, MO, USA) by determining the protein absorbance at 595 nm by a UV–Vis spectrophotometer (Shimadzu 3000, Kyoto, Japan). The solubility (%) was calculated according to equation (1).

$$\text{Solubility}\ (\%) = \frac{\text{Protein content in the supernatant}\ (\text{mg/mL})}{\text{Total protein content before centrifugation}\ (\text{mg/mL})} \times 100\% \quad (1)$$

2.4.4. Thioflavin T (ThT) fluorescence spectroscopy

Thioflavin T (ThT) fluorescence assays were conducted to detect secondary structural changes in FPI dispersions using a fluorescence spectrophotometer (RF-6000, Shimadzu, Kyoto, Japan) with an excitation wavelength λ_{ex} of 440 nm and an emission wavelength λ_{em} of 460–560 nm (Herneke, et al., 2021). Specifically, ThT solution (2 mM) was passed through a syringe filter (0.22 μm, ThermoFisher Scientific, USA). The FPI dispersions were first diluted to 0.01 wt% using Milli-Q water (pH 7), followed by mixing with 2 μL ThT solution and kept in the dark for 10 min at 20 °C. The background solution was prepared by adding 2 μL ThT to 2 mL Milli-Q water (pH 7).

2.4.5. Negative staining transmission electron microscopy (TEM)

The microstructures of various treated FPI were observed by negative staining TEM according to Cheng et al. (2022). The FPI dispersions (2.5 wt %) were diluted 50 times with Milli-Q water (pH 7). Afterwards, the diluted sample solution (20 μL) was transferred onto a formvar-coated copper TEM grid and stained with uranyl acetate (2%) for 3 min. Excess stain was subsequently rinsed with 20 μL Milli-Q water for 3 min. Finally, a filter paper was used to drain excess liquid from the copper grid. Micrographs were acquired by an electron microscope (NL-5600 MD, Philips, Eindhoven, The Netherlands) at an acceleration voltage of 60 kV.

2.4.6. Circular dichroism (CD) spectroscopy

Secondary structure of various untreated and treated FPI dispersions were probed by a Chirascan CD spectrometer (Applied Photophysics, UK) according to Dave et al. (2013). The FPI dispersions were diluted with Milli-Q water (pH 7) to 0.5 wt%. For a far ultraviolet (FUV) CD study, samples (~80 μL) were loaded to a quartz cell (a path length of 0.1 mm) (Hellma, Germany). FUV CD spectra were collected at 1 nm intervals for 0.5 s per point in a wavelength range of 180 nm–260 nm at ~20 °C. The values of the FUV spectra were averaged from 10 measurements. The near-UV spectrum (NUV, wavelength 250–350 nm) were recorded at ~20 °C after transferring ~2 mL samples into a 10 mm Quartz Suprasil cell (#100-QX, Hellma, Germany) for a total scan time of 40 s.

2.4.7. Determination of surface hydrophobicity

The surface hydrophobicity (H0) of various FPI samples (2.5 wt %) was measured by fluorescence spectrophotometry using 8-anilino-1-naphthalene sulphonate (ANS) as a fluorescence probe Luo, Cheng, Zhang, and Yang (2022). FPI dispersions (2.5 wt %) were diluted separately to concentrations of 62.5, 125, 250, and 500 μg/mL using 10 mM Tris-HCl buffer (pH 7). ANS solution (8.0 mM, 50 μL) was then added to each FPI solution (3 mL) and kept in the dark for 20 min at ~20 °C. A Shimadzu RF-6000 fluorescence spectrometer (Shimadzu, Kyoto, Japan) was employed to determine the fluorescence at 470 nm (emission) and 390 nm (excitation) with a 5 nm slit length. Fluorescence intensities after subtracting background (FPI samples without ANS) were plotted against FPI concentrations, and H0 was represented as an original slope determined from linear regression analysis (Kato & Nakai, 1980).

2.4.8. Small-angle neutron scattering (SANS)

The QUOKKA instrument at ANSTO in Sydney, Australia, with a *Q*-range of 0.003–0.4 $Å^{-1}$ was used for the SANS experiments (scattering wave vector $Q = (4\pi/\lambda)\sin(\theta)$, and λ is the neutron wavelength (Å) and 2θ is the scattering angle) (Gilbert, Schulz, & Noakes, 2006; Wood et al., 2018; Yang et al., 2022). Samples were prepared according to the same procedures as depicted in sections 2.2 and 2.3. Liquid samples were pipetted into demountable SANS samples cells (thickness: 1 mm). Gel samples thermally melted in an oven at 90 °C for 30 min, then transferred to SANS sample cells and incubated at ~20 °C for at least 5 h prior to SANS measurements to allow for gel network formation. Liquid samples (such as the 2.5 wt% and 10 wt% control samples and the CH-1 sample were transferred into quartz cuvettes (path length: 1 mm) and placed into a tumbler to avoid sample sedimentation, such as the 2.5 wt % and 10 wt% control samples and the CH-1 sample. SANS measurement of each sample lasts for approximately 3 h at 20 °C. SANS data were reduced using procedures developed in ANSTO (Kline, 2006) with algorithms embedded in commercial Igor Pro software (Wavemetrics, USA).

2.4.8.1. SANS data analysis.

The correlation length model (Hammouda et al., 2004) was used to fit the SANS scattering profiles (equation (2)):

$$I(Q) = \frac{A}{Q^n} + \frac{C}{1 + (Q\xi)^m} \quad (2)$$

Where n is the power law exponent of the power law scattering in the low *Q* region originating from protein aggregates. The ξ is the correlation length (particle size) of protein particles and m is the power law exponent of the power law scattering in the high *Q* region. A and C are scale constants for the first and second term, respectively. The SasView software (version 5.0.5, http://www.sasview.org/) was used for the modelling implementation.

2.5. Characterisation of FPI gels

2.5.1. Flowability of FPI gels

The flowability of FPI gels was examined by inverting glass bottles containing differently treated FPI dispersions (10 wt%) after storage at ~20 °C for 24 h. Afterwards, photos were taken to observe the flowability of the gels.

2.5.2. Determination of rheological properties of FPI gels

Rheological characteristics of various FPI gels were assessed by a Paar Physica rheometer (Anton Paar, MCR 301, Austria). A plate-plate geometry (diameter: 40 mm) with a gap of 1 mm was used throughout the test. The FPI gels were loaded onto the bottom plate of the rheometer using a plastic spatula and carefully trimmed around the edge of the sample if necessary. To avoid evaporation, samples were covered with mineral oil. The rheological tests were performed in accordance with the following protocol. First, to structurally recover the FPI gel after loading, a time lapse measurement at strain 1% and frequency 1 Hz was conducted over 120 min. A frequency sweep test (frequency: 0.01–100 Hz) was then performed at 1% strain to investigate the viscoelasticity of the gel network. Finally, as strain sweep test was conducted with the strain amplitude varying from 0.01 to 1000 % at a constant frequency of 1 Hz. Storage modulus (G') and loss modulus (G'') were determined throughout the test at 20 °C (Hu, et al., 2023). The thermoreversibility of TS-30 gel was assessed by recording G' and G'' at a fixed frequency 1 Hz and strain 1% during a temperature sweep test, in which the temperature was ramped from 20 °C to 80 °C at 2 °C/min and then hold at 80 °C for 10 min before being decreased from 80 °C to 20 °C at the same rate.

2.5.3. Viscosity measurements

Viscosity was determined following the same protocol as depicted in Section 2.5.2. Viscosity measurements were performed by applying a

shear rate sweep from 0.1 to 1000 s^{-1} and a reverse sweep from 1000 to 0.1 s^{-1}. The degree of protein aggregation was measured by the area (S) of the hysteresis defined by the shear rate incline and decline curves, which was calculated with Origin Pro software (v. 2020, Origin Lab, MA, USA) (Luo, Zhang, Palmer, Hemar, & Yang, 2021). Duplicate measurements were made for each sample at 20 °C.

2.5.4. Scanning electron microscopy (SEM) observations of FPI gels

SEM sample preparation and imaging were performed according to Goeden-Wood, Keasling, and Muller (2003) with slight modifications. FPI gels were cut into small pieces using a spatula and fixed overnight (~4 °C) in 0.1 M sodium cacodylate phosphate buffer containing 2.5% glutaraldehyde. After fixation, the gels were rinsed three times with 0.1 M sodium cacodylate phosphate buffer. Subsequently, the gels were dehydrated in aqueous ethanol solutions with increased ethanol concentrations (30, 50, 70, 80, 90, and 100% ethanol, v/v). Finally, the dried FPI gels obtained from lyophilization were cut to ~1 mm × 1 mm in size. The gel samples were coated with gold for 240 s at 12 mA at ~20 °C. SEM images were acquired at 5 kV using a scanning electron microscope (Philips XL 30 S FEG, Eindhoven, The Netherlands).

2.6. Formation and characterisation of FPI stabilised emulsions

2.6.1. Interfacial tension measurements

A Theta Flex Plus optical tensiometer (Biolin Scientific Instruments, Sweden) built on the pendant drop principle was used to monitor interfacial tension at O/W interface up to 6000 s (Hu, et al., 2023). A drop of selected FPI samples after treatments (25 μL) was formed at the tip of a stainless-steel syringe needle and immersed in soybean oil. The data was processed using One Attention software (Biolin Scientific Instruments, Sweden).

2.6.2. Preparation of emulsions

FPI-stabilised emulsions were made by homogenising different concentrations of control and TS-30 FPI solutions (1, 3, and 5 wt %) with soybean oil at various oil-phase volume fractions ($\varphi = 0.2–0.7$, v/v). An Ultra-Turrax rotor stator mixer (T10 basic, IKA Corp., Staufen, Germany) equipped with a 10 mm probe (S10N-10 G, IKA, Germany) was used to homogenise the oil-water mixture at 20,000 rpm for 2 min. Emulsions prepared from FPI dispersions without any treatment were used as controls.

2.6.3. Determination of oil droplet sizes

A Mastersizer instrument (Malvern Instruments Ltd, Worcestershire, UK) was employed to determine the average particle size distribution (PSD) of oil droplets as described by Hu et al. (2023). The refractive indices used for soybean oil and dispersant (Milli-Q water) were 1.47 and 1.33, respectively (da Silva, Almeida, & Sato, 2021). Sauter mean diameter (D [3,2]) was used to indicate the mean size of oil droplets (in diameter), and changes in droplet size were also monitored over 28 days at 20 °C.

2.6.4. Rheological measurements of emulsions

Rheological tests were conducted following the same methodology as depicted in section 2.5.2. Data were collected at 20 °C, and G' and G'' were recorded throughout a frequency sweep (ranging from 0.01 to 100 Hz at 1% strain) and strain sweep test (ranging from 0.1 to 1000% at 1 Hz frequency). Viscosity determinations were also conducted at a shear rate increased from 0.1 to 1000 s^{-1} and then declined from 1000 to 0.1 s^{-1} at 20 °C.

2.6.5. Microstructures of emulsions

The emulsions were imaged by a light microscope (BX53, Olympus, Japan) equipped with a × 40 objective lens. After gently inverting the emulsion samples 3–5 times, the emulsions were transferred on a microscope slide and covered. Observations were performed in triplicate, and representative images are shown. To visualise the interfacial structures at the oil-water interface, confocal laser scanning microscopy (CLSM) was applied to selected samples. Fast Green (1% w/v, ratio to emulsion 1:500 (v/v)) and Nile Red (ratio to emulsion 1:5000 (v/w)) was utilized to stain protein and oil phases of emulsions, respectively (Hu, et al., 2023). Afterwards, aliquots of the emulsion samples were loaded on a glass slide with a cavity. The edges of slides were then carefully enclosed with nail polish to minimise water evaporation. A confocal laser scanning microscope (Leica DM 6000 B, Germany) equipped with an oil immersed 100 × objective lens was utilized to observe emulsions at laser wavelengths of 633 nm (Fast green) and 561 nm (Nile red). Optical light and CSLM micrographs were analysed by using Image J software (NIH, MD, USA).

2.6.6. Creaming index

Emulsion stability was assessed visually according to Wynnychuk et al. (2021), including observation of the occurrence of phase separation or coalescence in emulsions. The creaming index was calculated from Equation (3).

$$Creaming\ index = \left(\frac{H_s}{H_0}\right) \times 100\% \quad (3)$$

where H_s is the height of serum measured, and H_0 is the height of the emulsion. Therefore, a smaller creaming index indicates emulsions with a higher creaming stability.

2.7. Statistical analysis

At least duplicate measurements for conducted for each characterisation, and the results are shown as average with standard deviation (SD). The statistical analysis was conducted using Minitab statistical software (version 19, USA), and a one-way analysis of variance (ANOVA) was employed to assess mean differences with a significance level of $P < 0.05$ according to Tukey's test.

3. Results and discussion

3.1. FPI protein profiles by SDS-PAGE

SDS-PAGE was performed to reveal modifications in FPI protein profiles as affected by TS or CH treatments (Fig. 1). In non-reducing SDS-PAGE (Fig. 1A), a profound and smeared protein band were identified in the loading wells for all the samples, suggesting the existence of large protein complexes with molecular mases greater than 250 kDa (Kaspchak, et al., 2017). Additionally, the native FPI (control) exhibits a complicated protein profile consisting of two dominant protein bands locating at ~70 kDa and ~50 kDa, which are assigned as convicilin and vicilin, respectively (Vogelsang-O'Dwyer et al., 2020). Some small proteins at ~37 kDa and ~20 kDa are assigned to α-legumin and β-legumin, respectively (Langton, et al., 2020). This protein profile of native FPI is consistent with previous studies (Hu, et al., 2023; Nivala, Mäkinen, Kruus, Nordlund, & Ercili-Cura, 2017; Vogelsang-O'Dwyer et al., 2020).

Application of TS or CH treatment significantly reduced the densities of protein bands (40–70 kDa, 30–37 kDa, and 15–20 kDa) compared to untreated FPI. (Fig. 1A). Similar results were found in heat-treated FPI (70 °C, 30 min) at pH 7 (Alavi, Chen, Wang, & Emam-Djomeh, 2021) and TS-treated mung bean protein (70 °C, 30 min) at pH 7 (Zhong & Xiong, 2020). Moreover, with increasing treatment time in either CH or TS treatment, the fading of protein bands in particular at 40–70 kDa became more significant, indicating that more severe treatment at longer times induces more extensive intermolecular bond formation (Luo, et al., 2021; Zhong & Xiong, 2020). For example, it can be observed that the CH-8 sample (conventional heating for 8 h) exhibited the lowest density for all protein bands. Previous studies suggested that

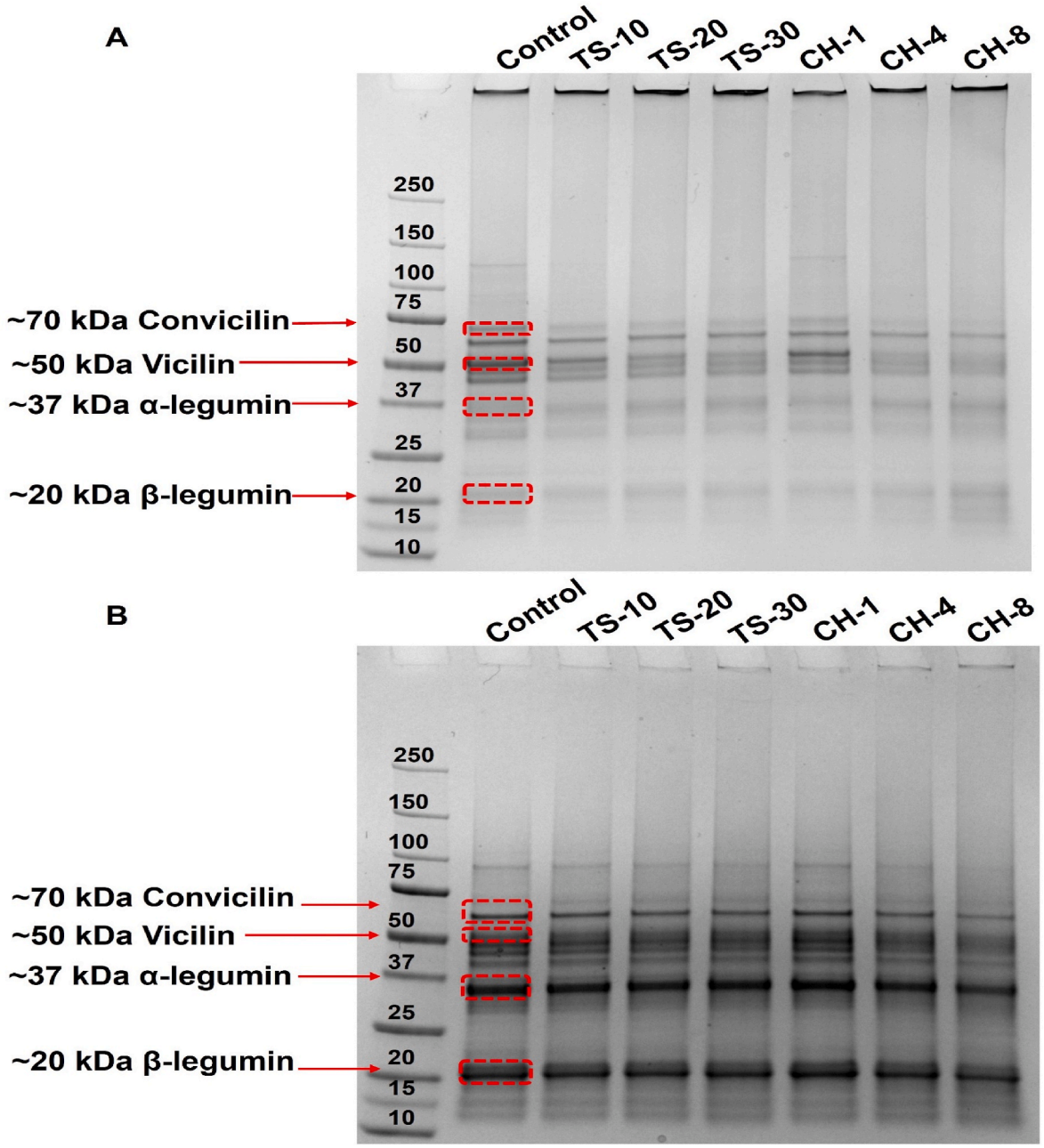

Fig. 1. SDS-PAGE patterns of faba bean protein isolates (FPI) dispersions at pH 7 before and after thermosonication (TS) (10, 20, and 30 min) or conventional heat treatment (CH) (90 °C, 1 h, 4 h, and 8 h) under non-reducing (A) and reducing (B) conditions.

the effect of CH and TS processing on the degree of protein aggregation is highly dependent on the treatment temperature and time (Speroni, et al., 2009).

Under reducing conditions, the large protein aggregates observed in the loading wells disappeared (Fig. 1B), indicating that they were mainly stabilised by disulfide bond. In addition, all FPI dispersions show similar protein profiles, which is consistent with a previous TS study on mung bean proteins (Zhong et al., 2020). Additionally, for all samples, densities of protein bands at ~37 kDa (α-legumin) and ~20 kDa (β-legumin) became much denser under reducing conditions, suggesting that these two legume subunits were associated via disulfide bonds (Hu, et al., 2023). In CH-8 FPI sample, a decrease in densities of all protein bands (<150 kDa) was seen, which could be due to production of protein aggregates with a low solubility (Luo, Yang, et al., 2022).

3.2. *Effect of CH and TS treatments on physicochemical peroperties of FPI dispersions*

3.2.1. *Visual appearance*

The appearance of the FPI dispersions (2.5 wt%) and gels (10 wt%) after TS and CH is shown in Fig. 2A. For 2.5 wt% FPI, the control and CH-treated samples showed significant turbidity, and protein sedimentation was observed at the bottom of glass vials, as indicated by the red arrow (Fig. 2A). This could be due to the low solubility of FPI and protein aggregation after CH (Alavi, Chen, & Emam-Djomeh, 2021; Alavi, Chen, Wang, & Emam-Djomeh, 2021). After TS treatment (10–30 min), the FPI dispersions became translucent. Furthermore, at a high protein concentration (10 wt%), all TS and CS treatments induced formation of self-supporting gels (Fig. 2A). The rheological and microstructural properties of FPI gels induced by different treatments were further investigated in **Section 3.6**.

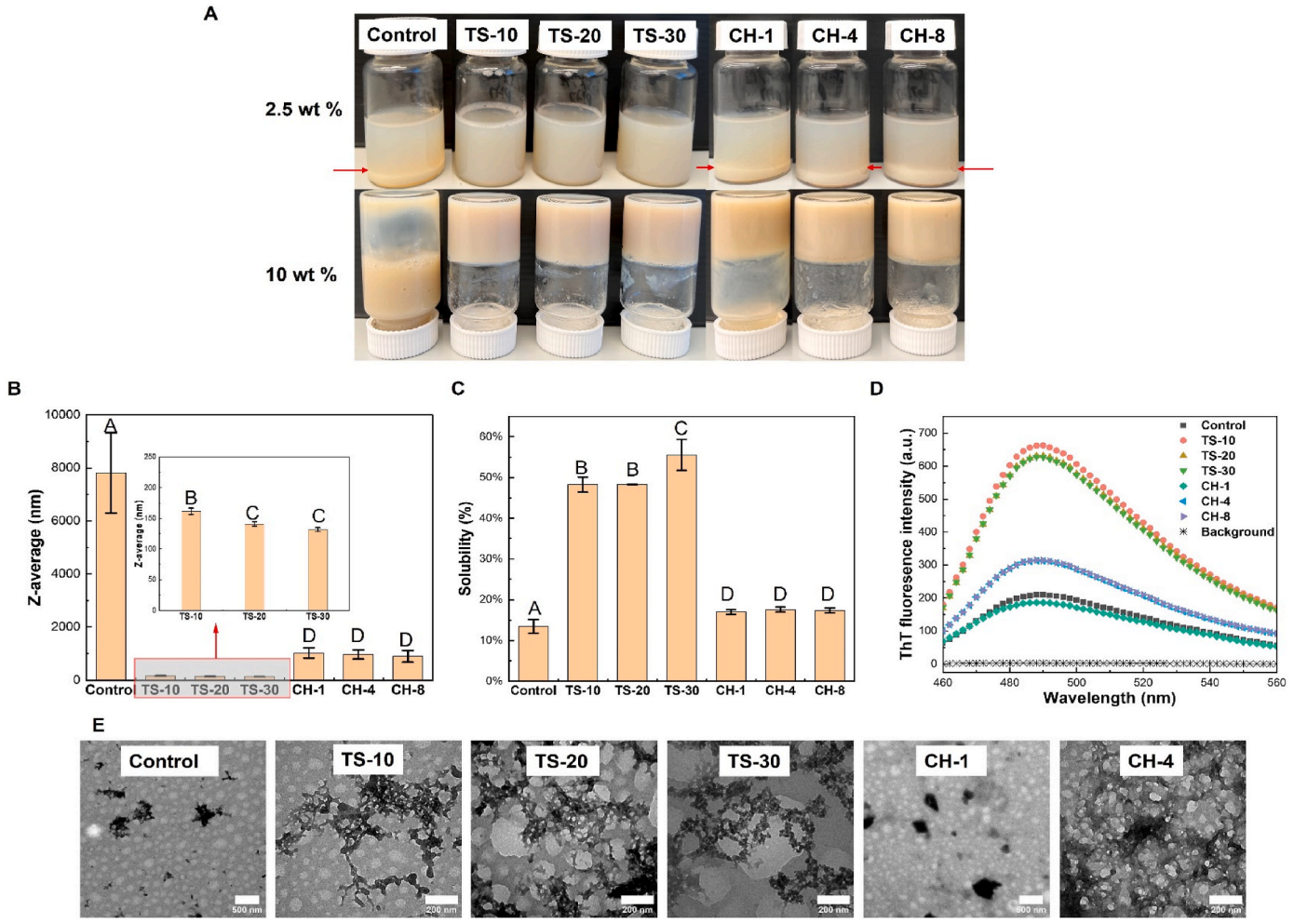

Fig. 2. (A) Visual appearance of 2.5 wt% and 10 wt% faba bean protein isolate (FPI) samples before and after thermosonication (TS) or conventional heat treatment (CH) for different times at pH 7. (B) Particle size (z-average) of control and TS- or CH-treated FPI dispersions at pH 7. (C) Solubility of control and TS- or CH-treated FPI dispersions at pH 7. (D) ThT fluorescence spectra of various FPI samples before and after TS (10, 20, and 30 min) or CH treatments (1, 4, and 8 h) at pH 7. (E) TEM images of FPI dispersions before and after TS (10, 20, and 30 min) and CH (1 and 4 h) at pH 7. Different letters above the columns indicate significant differences ($P < 0.05$).

3.2.2. *Particles sizes and solubilities of FPI affected by TS and CH*

The particle size and solubility of control, CH- and TS- treated FPI dispersions (2.5 wt %) at pH 7 are demonstrated in Fig. 2B and C. The control sample exhibits the largest particle size (~7800 nm) and the lowest solubility (~13.43%) among all samples. Previous studies showed that most native and untreated plant proteins have the largest particle size and lowest solubility, such as quinoa protein isolates (QPI) before sonication (Luo, Yang, et al., 2022) and soy protein isolate (SPI) before pH shifting (Fang, et al., 2021). This could be typically caused by protein aggregation during isoelectric point precipitation after alkaline extraction (Grossmann & McClements, 2023). TS treatment induced a significant reduction in particle size from ~7800 nm (Control) to ~140 nm (TS-30) at pH 7 (Fig. 2B). Previous studies suggested that some protein interactions, such as hydrophobic interactions and hydrogen bonds, may be destroyed by the combination of heating and sonication, resulting in smaller particle size and higher solubility (Frydenberg, Hammershøj, Andersen, Greve, & Wiking, 2016; Zhu et al., 2023). This was further confirmed with the solubility results showing that FPI solubility remarkably increased from ~12% (control) to ~55% (TS-30) (Fig. 2C). The improvement in FPI solubility could be associated with creation of hydrogen bonds between water and protein after TS, which improved protein solubilization by replacing the intramolecular hydrogen bonds in protein molecules (Jiang, et al., 2017). Zhong and Xiong (2020) also reported that TS significantly improved the solubility of mung bean protein dispersions at different temperatures (e.g. 30, 50, and 70 °C) for 5–30 min and the solubility improved with an increase in treatment temperature and time.

Compared to untreated FPI (Control), CH-treated samples had reduced particle size (from ~7800 to ~1000 nm) which did not change significantly with increased CH time (Fig. 2B). Similar results were reported for heated SPI (Ó Flynn et al., 2021) and egg white proteins (Sponton, Perez, Ramel, & Santiago, 2017), which could be due to partial protein dissociation at high temperature. In addition, compared to the native sample, the solubility of the CH-treated FPI samples increased slightly to ~17% (Fig. 2C). A similar observation has been made previously for SPI after heat treatment (90 °C, 20 min). This could be attributed to a decreased protein particle size and alterations of various non-covalent and covalent interactions under heat treatment, thereby affecting protein conformations and their hydration capabilities (Ó Flynn et al., 2021; Zhao, Xiong, Chen, Zhu, & Wang, 2020).

3.2.3. *Thioflavin T (ThT) fluorescence assay*

To identify the formation of FPI aggregates after various treatments, thioflavin-T (ThT) fluorescence experiments were conducted. ThT can specifically attach to the β-sheet surface, giving rise to higher fluorescence intensity (Biancalana & Koide, 2010; Stathopulos et al., 2004). In Fig. 2D, compared to the background, all TS-treated FPI samples show a significant increase in ThT fluorescence with a peak intensity at ~480

nm, which suggests that protein aggregates containing β-sheet were formed after TS. Similar findings were reported by Chen et al. (2019), who also identified that the ThT intensity of peanut protein was significantly enhanced after a TS treatment (72 °C, 500 s) at pH 7. In addition, Fig. 2D shows a slight increase in ThT fluorescent intensity in CH-4 and CH-8 samples compared to the untreated FPI (control), indicating an increase in β-sheet structure formation after prolonged heating. A comparable result has been reported in a previous FTIR study on lentil proteins after a 16 h heat treatment at 90 °C. It has been suggested that the prolonged heating could promote protein unfolding followed by formation of protein aggregates that are rich in β-sheet secondary structures (Jo, et al., 2020). However, the lowest ThT fluorescence intensity was found in the CH-1 sample. This could be related to protein aggregation, which reduces the surface area available for ThT binding (Hu, et al., 2023; Jo et al., 2020; Josefsson et al., 2019).

3.2.4. *Morphology of FPI aggregates as revealed by TEM*

TEM images of untreated and treated FPI (TS or CH) samples are shown in Fig. 2E. The untreated (control) FPI showed submicron scale particle aggregates. In comparison, after 10 min of TS treatment, an interconnected protein network with clusters of loosely packed FPI aggregates can be observed, contributing to an increase in ThT fluorescence intensity shown in Fig. 2D. As the TS time increases to 20 and 30 min, more and denser interconnected protein aggregate network can be observed. CH treatment also induced significant structural changes of FPI. At shorter heating times (e.g., CH-1), large and dense protein

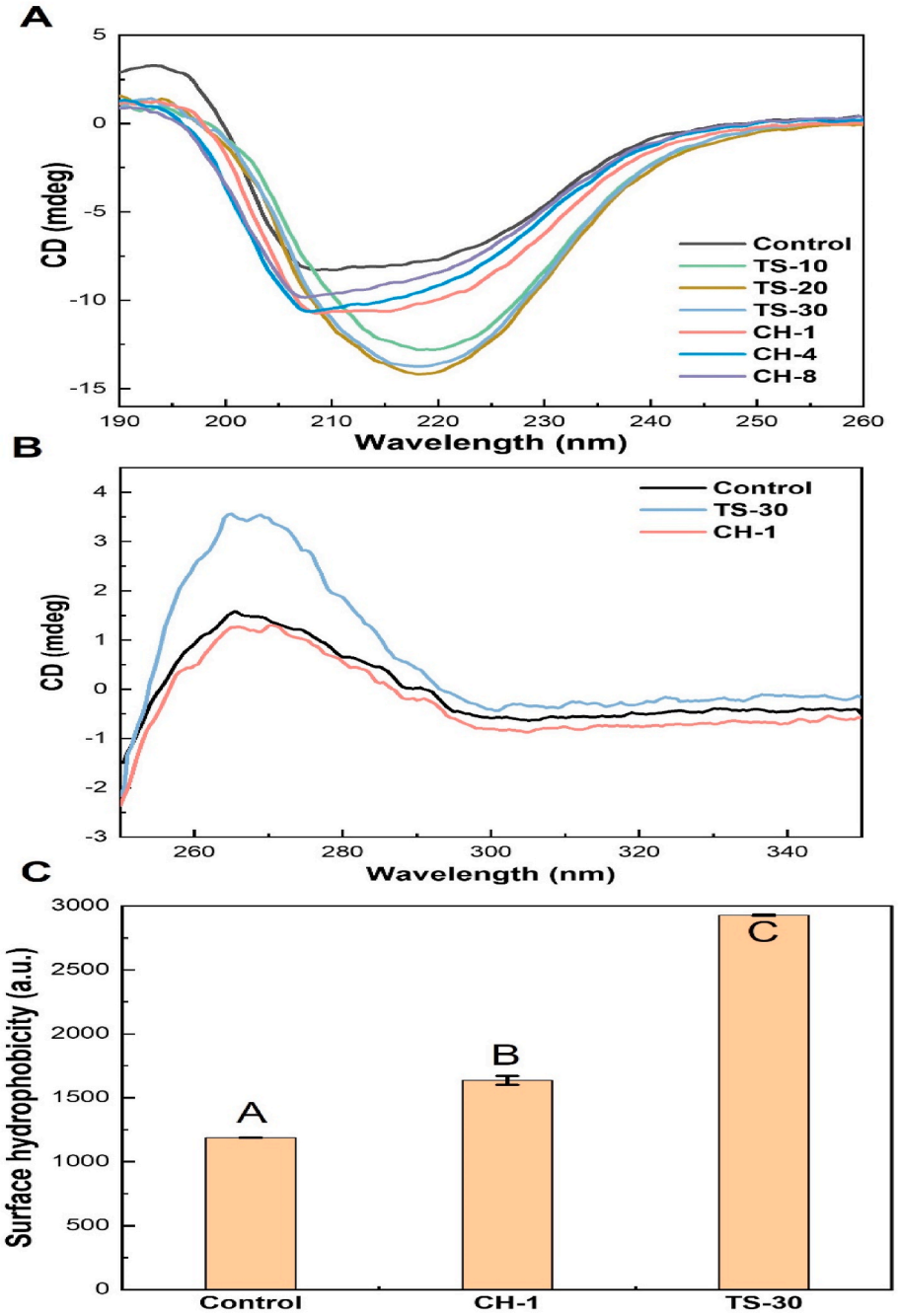

Fig. 3. (A) Far ultraviolet (UV) circular dichroism (CD) spectra of faba bean protein isolate (FPI) dispersions before and after thermosonication (TS) (10, 20, and 30 min) or conventional heat treatment (CH) (1–8 h) at pH 7; (B) Near-UV CD spectra of untreated and selected TS- (30 min) or CH- (1 h) treated FPI samples (TS-30 and CH-1). (C) Surface hydrophobicity of untreated and selected TS- or CH-treated FPI samples (TS-30 and CH-1).

aggregates can be observed, consistent with the low ThT fluorescence intensity (Fig. 2D). On the other hand, the formation of interconnected FPI aggregates was observed after heating FPI for longer heating times (CH-4). Similar microstructures have been reported in lentil protein dispersions after a prolonged heating at pH 7 (Jo, et al., 2020). Combined with the findings of SDS-PAGE and ThT fluorescence, TS treatment and prolonged heating under neutral conditions (pH 7) causes FPI to denature and aggregate by disulfide bond formation and non-covalent interactions (Fig. 1) (Jiang, et al., 2017; Luo, Yang, et al., 2022). These protein aggregates could undergo further structural rearrangement to form fibril-like FPI aggregates through the formation of β-sheet structures, which play an important role in stabilising fibrillar like structures (Chen, et al., 2019; Kong & Yu, 2007).

3.3. Changes in protein secondary structures probed by CD spectra

Fig. 3A demonstrates the far-UV CD spectra of FPI treated by TS or CH. The native FPI (Control) samples exhibited a molar ellipticity positive peak at ~195 nm, and another two negative minimums at ~206 nm and ~220 nm, respectively. These peaks indicate that the secondary structure of native FPI at pH 7 is dominated by random coils, α-helices, and β-sheets (Gülseren, Güzey, Bruce, & Weiss, 2007), similar to a previous study (Nivala, Nordlund, Kruus, & Ercili-Cura, 2021). In Fig. 3A, the peak change for the CH-treated FPI samples was not significant, and the secondary structure of the CH-treated FPI samples showed native-like shapes with a slightly strengthened peak at ~206 nm and a weakened peak at ~220 nm. The slight increase in intensities ~220 nm could indicate an increase in β-sheet structure, which agrees well with the ThT results (Fig. 2D).

Conversely, in the far-UV CD spectra of TS-treated FPI (Fig. 3A), the negative peak of native FPI at ~206 nm was red shifted to ~218–220 nm with a remarkable increase in peak intensity, indicating an increased β-sheet secondary structures after the TS treatment (Greenfield, 2006; Kutzli, Zhou, Li, Baier, & Mezzenga, 2023). This finding agrees well with the ThT fluorescence results. The dominated β-sheet secondary structures have been also observed in TS-treated peanut protein isolate (Chen, et al., 2019) and mung bean protein (Zhong & Xiong, 2020). Compared to ultrasonication alone, the TS treatment with combination of heat and ultrasound could generate more intensive and steady acoustic cavitation field, leading to extensive protein denaturation and unfolding (Chen, et al., 2019; Villamiel & de Jong, 2000). Under certain circumstances, the unfolded protein molecules structurally rearranged to produce secondary structures (i.e. β-sheets) with a higher thermodynamic stability (Kong et al., 2007; Lefevre & Subirade, 2000).

To determine the tertiary structure changes after CH or TS treatment, the near-UV CD spectra of native FPI (control), TS- and CH-treated FPI were also recorded (Fig. 3B). In general, the near-UV CD spectra indicated the number of aromatic amino acids of proteins and associated mobility as well as their interactions (e.g. hydrophobic bonds) (Fasman, 2013). As demonstrated in Fig. 3B, native FPI had a significant positive dichroic peak at ~270 nm, indicating the presence of accumulated tyrosine residues (Yang et al., 1986). For the CH-1 sample, the magnitude of the positive peak at ~270 nm decreased slightly, suggesting a little impact on tertiary structure of FPI; the slight decrease in dichroic intensity could be due to protein aggregation. This is consistent with ThT fluorescence results (Fig. 2D). However, the magnitude of this peak increased substantially after 30 min of TS, suggesting the formation of a more well-defined and stable tertiary structure (Tang, Wang, & Huang, 2012).

3.4. Surface hydrophobicity

The surface hydrophobicity of untreated (Control), CH- and TS-treated FPI samples is shown in Fig. 3C. The surface hydrophobicity of FPI samples increased significantly after CH- or TS-treatment (from ~1187 to ~1635 after CH and ~2927 after TS). The largest increase in hydrophobicity was found in the TS-treated samples, which could be due to a significant exposure of interior hydrophobic groups caused by unfolding of protein molecules (Hernoux Villière, Lassi, & Lévêque, 2013). Although there was a slight rise in surface hydrophobicity after CH treatment compared to untreated FPI, the surface hydrophobicity of CH samples was still significantly lower than TS samples (Fig. 3C), which could be attributed to the limited exposure of initially buried hydrophobic groups after heat treatment only (Voutsinas, Cheung, & Nakai, 1983; Zhao et al., 2020). This observation was also in accordance with Guo et al. (2015) and Wang, Li, Jiang, Qi, and Zhou (2014), who showed that the surface hydrophobicity of SPI slightly increased after heating at 90 °C for 30–60 min.

3.5. Small-angle neutron scattering (SANS) analysis

The nanostructure of various treated FPI dispersions and hydrogels were further investigated by SANS (Fig. 4). In Fig. 4A, the scattering intensity I (Q) at low Q ($6 \times 10^{-4} < Q$ ($Å^{-1}$) $< 2 \times 10^{-2}$) of the TS-30 sample (2.5 wt% FPI) was greater compared to that of the native FPI (2.5 wt%), and the shape of the scattering pattern was also significantly changed after TS, indicating the microstructure of FPI was dramatically changed. The increase in the scattering intensity could be due to large nanoscale protein aggregates induced by the TS treatment. In addition, a greater scattering intensity was also observed in the higher concentration (10 wt% TS-30 and CH-1) FPI samples, which could be due to more considerable protein aggregation and gel network formation (Napieraj, et al., 2022). A correlation length model (**equation (2)**) was utilized to fit SANS profiles and fitting parameters are summarized in Table 1. Specifically, in the low Q region, all samples exhibited a Porod exponent (n) in a range of 2.3–2.6, which is a characteristic of mass fractal structures. The differences in the low-Q Porod exponent (n) suggest different large scale structural arrangement in FPI as affected by TS or CH treatment (Yang, et al., 2016). The Lorentz exponent, m of all the FPI samples is ~4.0, indicating a relative sharp interface between protein particles and solvent (Boukari, Lin, & Harris, 1997).

The largest structural difference among different FPI samples is the correlation length (ξ), representing structural inhomogeneities or nanoaggregates within protein aggregates or gel networks (Banc, et al., 2016). From Table 1, TS-30 treatment induced a substantial increase in the correlation length (ξ) compared to control and CH-1 samples. These structural inhomogeneities with a size of 120–144 Å may indicate the size of protein aggregates, confirming that the TS treatment is efficient to induce FPI protein unfolding and aggregation which agrees with the SDS-PAGE and TEM findings.

3.6. Characterisation of FPI gels

3.6.1. Small and large deformation rheological properties of various FPI gels

Gelation and rheological behaviour are among one of the most important properties of plant proteins (Akharume, Aluko, & Adedeji, 2021; Loveday, 2019). The frequency dependent viscoelastic properties of FPI gels induced by TS or CH treatments are shown in Fig. 5A. The G' and G'' of all samples were parallel to each other and only slight changes were observed with frequency. This indicates that all treated FPI samples had prevailing elastic and solid-like behaviours (Banerjee & Bhattacharya, 2012; Wei & Huang, 2020). This agrees well with the visual observation in Fig. 1A, which shows a self-supporting 10 wt % FPI hydrogel formed at pH 7 after TS treatment (10–30 min) and CH treatment (1–4 h).

To better compare gel strengths between FPI gels induced by different treatments, the G' (1 Hz) is plotted in Fig. 5C for all samples. CH-treated FPI gels showed significantly larger G' (1 Hz) values compared to TS-induced gels after prolonged heat treatment, suggesting that heat treatment (>1 h) is more effective in facilitating formation of FPI gel network. The longer the CH time, the greater the gel strength.

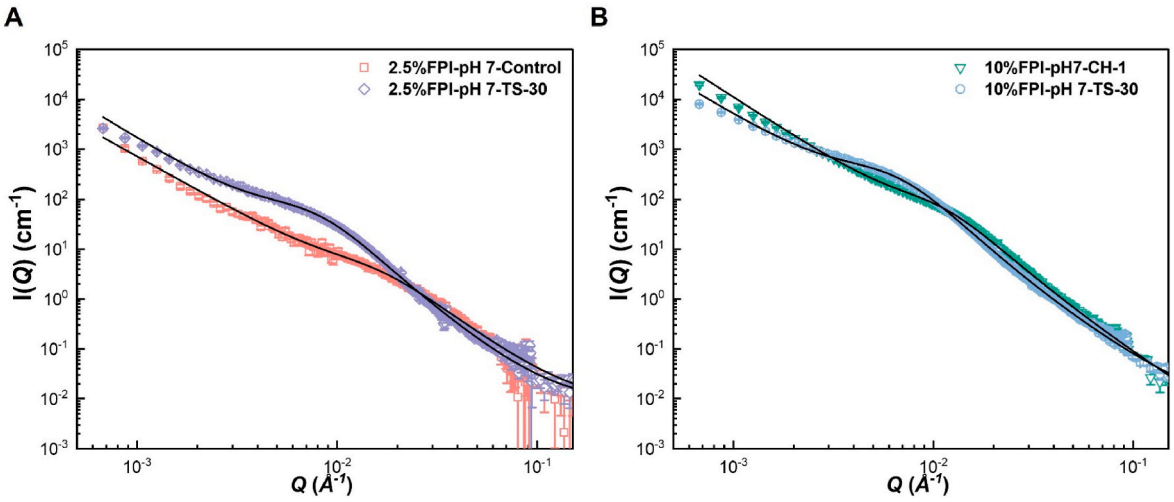

Fig. 4. Small-angle neutron scattering (SANS) profiles of (A) faba bean protein isolate (FPI) (2.5 wt%) dispersions before and after thermosonication (TS) treatment for 30 min (TS-30) at pH 7 (B) FPI gels (10 wt%) induced by TS treatment for 30 min (TS-30) or conventional heat treatment (CH) for 1 h (CH-1) at pH 7. The solid black lines are the correlation length model fits to the scattering data (eq (2)).

Table 1
SANS model fit structural parameters of faba bean protein isolate (FPI) dispersions (2.5 wt%) and gels (10 wt%) as affected by thermosonciation treatment for 30 min (TS-30) or conventional heat treatment for 1 h (CH-1).

Samples	Porod exponent, n	Correlation length, ξ (Å)	Lorentzian exponent, m
2.5 wt% FPI-control	2.3 (0.1)	60 (5)	4.0 (0.1)
2.5 wt% FPI-TS-30	2.5 (0.1)	120 (2)	4.0 (0.1)
10 wt% FPI-TS-30	2.5 (0.1)	144 (3)	4.0 (0.1)
10 wt% FPI-CH-1	2.6 (0.1)	87 (3)	4.0 (0.1)

Numbers in parentheses represent error bars.

Specifically. G' (1 Hz) increased from ~150 Pa (CH-1) to ~1255 Pa (CH-8) with increasing CH time. Similar findings have been observed with other plant proteins. For example, a two folds increase in gel strength was found for lentil proteins after heating at 90 °C from 1 h to 16 h. The prolonged heating above the protein denaturation temperature could substantially facilitate the disintegration of protein molecules and exposure of the initially buried hydrophobic groups, thereby facilitating interactions between proteins and subsequent gel network formation (Jo, et al., 2020). TS treatment could also induce the formation of FPI gels even within a very short time (e.g. 10 min), showing its high potential as a novel gel formation method. However, the G' (1 Hz) of the TS-induced FPI gels (Fig. 5A and C) gradually decreased as the TS time increased from 10-min TS (~372 Pa) to 30-min TS (~289 Pa). This effect may have arisen from over-exposure of the molecules to acoustic cavitation by sonication, which breaks down protein chains, disrupts protein association, and impairs further aggregation (Hu, Li-Chan, Wan, Tian, & Pan, 2013; Khatkar, Kaur, & Khatkar, 2020).

Strain-sweep test was used to measure the strain dependent rheological behaviour and structural yield characteristic of FPI gels formed after TS or CH treatments (Fig. 5B). Quantitatively similar strain dependent behaviours were observed in all FPI gels. At the small strain amplitude that was within the linear viscoelastic region (LVR), both G' and G'' were constant with an increase in strain amplitude, indicating a typical characteristic of linear viscoelastic behaviour. Furthermore, within the linear viscoelastic region (LVR), the value of G' was greater than G'', suggesting a prevailing elastic behaviour with a solid-like structure consistent with visual appearance and frequency sweep measurements (Munialo, Martin, Van Der Linden, & De Jongh, 2014). When the strain amplitude was further increased above the LVR, a sharp drop in G' was observed in all FPI gels due to structural disintegration (Yang, et al., 2022). As for the value of G'', when the strain increased above the LVR, it initially increased to a maximum and then decreased remarkedly with further increases in strain; this can be categorised as type III nonlinear rheological (weak strain overshoot) behaviour (Hyun, Kim, Ahn, & Lee, 2002). The overshoot of G'' could be due to structural rearrangement under large shear deformation (Hyun, et al., 2002). Similar large deformation rheological behaviour has been observed for hydrogels made from other plant proteins such as soybean protein (Xia, Siu, & Sagis, 2021) and pea protein (Wittek, Walther, Karbstein, & Emin, 2021).

As the further increase in strain amplitude, crossover of G' and G'' was observed and the strain and stress values at that point can be identified as the breaking strain and breaking stress, respectively. After passing this point, the G'' value is higher than G', indicating the sample began to flow due to significant structural disintegration (Yang, et al., 2016). The values of breaking stress (σ_b) and breaking strain (γ_b) are shown in Fig. 5D. For CH induced FPI gels, the σ_b increased with treatment time (from ~60 to ~341 Pa), but with increasing TS treatment time, the σ_b gradually decreased following a similar trend (from ~128 to ~95 Pa) as G' at 1 Hz (Fig. 5C). However, FPI gels induced by TS treatments showed similar γ_b values with the longer treatment time (Fig. 5D). The γ_b values of TS-treated FPI gels ranged from ~29 to 33%, which were similar to the γ_b value of ~34% for CH-4 FPI gels. This indicates that TS treatment can effectively form FPI gels with similar resistance to larger shear deformation before breakdown using a shorter treatment time than CH treatment.

3.6.2. *Viscosity of various FPI gels*

The flow curves of control, CH- and TS-treated 10 wt % FPI dispersions at pH 7 are shown in Fig. 5E. Shear-thinning behaviour was observed in all samples with viscosity decreasing with increasing shear rate. This has been widely reported in plant protein gels, including SPI gels (Ningtyas, Tam, Bhandari, & Prakash, 2021), pea protein gels (Beck, Knoerzer, Sellahewa, Emin, & Arcot, 2017), and quinoa proteins (Luo, et al., 2021). Compared to the control, CH or TS-treated FPI samples showed significantly higher viscosity, following the trend of G' at 1 Hz (Fig. 5C). The viscosity values at 10 s^{-1} are plotted in Fig. 5F, in which the control and CH-1 samples had significantly lower viscosity at 10 s^{-1} than the other treated samples; this is consistent with the visual observation in Fig. 2A. Similarly, TS samples had a similar viscosity range of

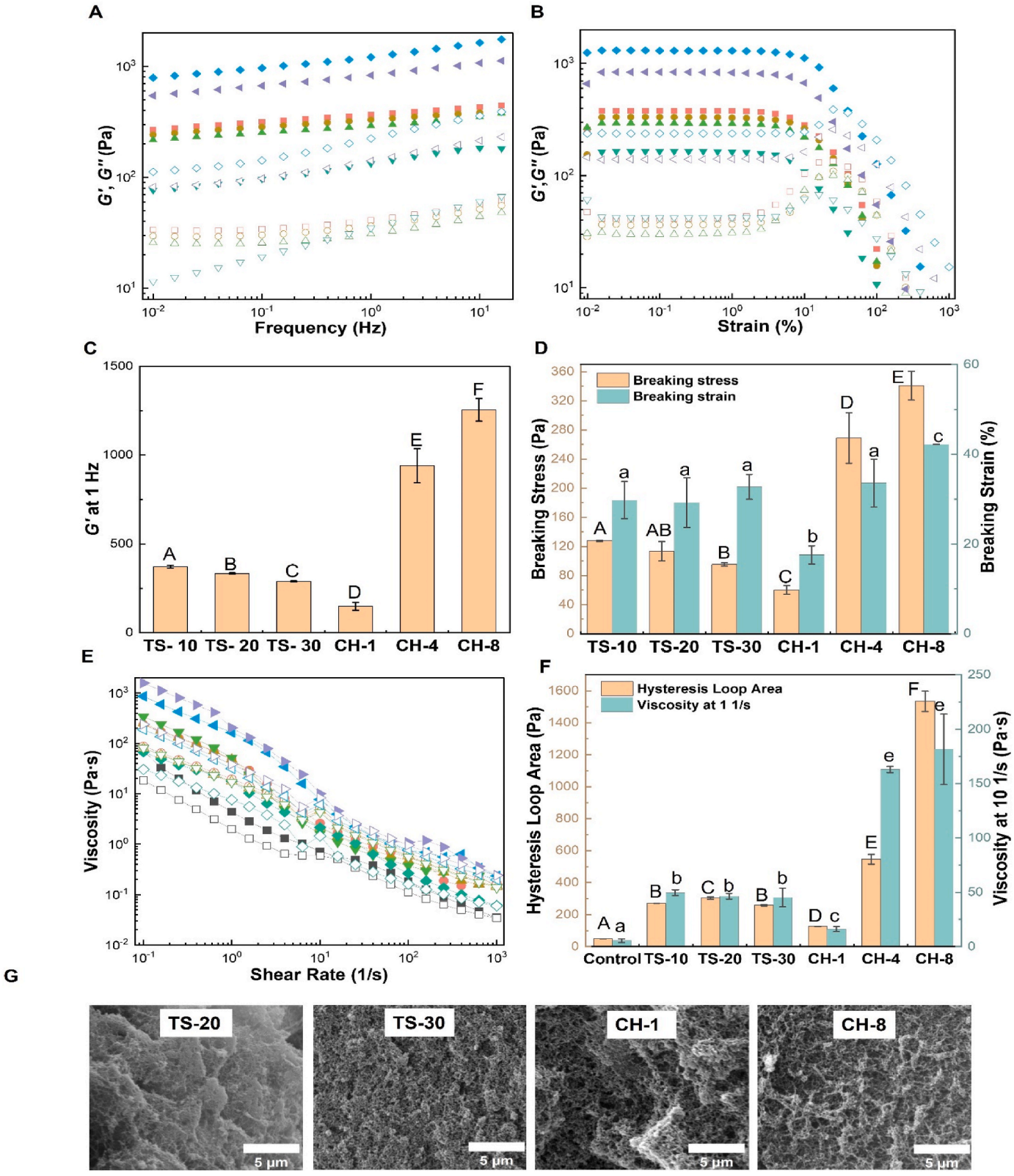

Fig. 5. Storage modulus (G', solid symbols) and loss modulus (G'', empty symbols) as a function of frequency (A) and strain amplitude (B) for faba bean protein isolate (FPI) gels induced by thermosonication (TS) or conventional heat treatment (CH). Symbols correspond to: TS-10 (■),TS-20 (●),TS-30 (▲), CH-1 (▼),CH-4 (◀), and CH-8 (◆). (C) Gel strength (G' at 1 Hz) and (D) breaking strain (γ_b) and breaking stress (σ_b) for various FPI gels induced by thermosonication (TS) or conventional heating treatment (CH). (E) Viscosity as a function of shear rate for various untreated and treated FPI dispersions (10 wt%, pH 7). Solid and open symbols represent the "up" and "down" measurements, respectively. Symbols correspond to: Control (■), TS-10 (●), TS-20 (▲), TS-30 (▼),CH-1 (◆), CH-4 (◀), and CH-8 (▶). (F) Thixotropic hysteresis loop area and viscosity at 10 s^{-1} of TS- and CH-treated FPI dispersions (10 wt%, pH 7)obtained from the "up" and "down" viscosity measurements. (G) SEM images of selected FPI (10 wt%, pH 7) gels induced by thermosonication (TS) for 20 min (TS-20) and 30 min (TS-30) or conventional heating treatment (CH) for 1 h (CH-1) and 8 h (CH-8). In (C, D, and F) different superscript letters above the column denote significant differences ($P < 0.05$).

~46–~49 Pa•s, which was not significantly affected by TS time. For CH-treated samples, the viscosity increased dramatically when the heating time was increased from 1 h (~130 Pa•s) to 8 h (~1500 Pa•s).

Fig. 5E shows the "up" and "down" viscosity sweep tests. All samples had lower viscosity in "up" measurement than in "down" measurement. The consequent hysteresis loop indicates that these samples are thixotropic and suggests a time-dependent flow behaviour (Armelin, et al., 2006). The thixotropy was indicated by determination the area between the up and down curves (hysteresis) in Fig. 5E with larger areas indicating stronger thixotropic behaviour as shown in Fig. 5F (Armelin, et al., 2006; Luo et al., 2021). Basically, the trend of hysteresis loop area among samples was consistent with the viscosity at 10 s^{-1} (Fig. 5E). Briefly, the CH-8 sample had the largest hysteresis loop area (~1535 Pa), while the TS-treated samples had a similar area ranging from ~259 to ~304 Pa. FPI gels that require higher energy to break the internal structure are expected to result in greater hysteresis. This finding is in line with the rheological behaviour and will be further discussed in the context of microstructural characteristics below.

3.6.3. SEM imaging of FPI gels

The microstructure of selected FPI gels induced by TS (20 and 30 min) and CH (1 and 8 h) was observed by SEM (Fig. 5G). The CH-treated samples exhibited large irregular pores with non-homogeneous spatial structure. Specifically, the CH-8 sample exhibited a cross-linked protein network structure with thicker strands compared to the other samples, which explains its greater gel strength and larger extent of thixotropic behaviour. With prolonged heating time (4 and 8 h), FPI molecules unfolded more sufficiently so that active groups of proteins were extensively exposed, subsequently forming stronger gel networks (Jo, et al., 2020). Similar gel microstructures have been reported in a previous SEM investigation of lentil protein gels induced by prolonged heating (Jo, et al., 2020). In contrast, an uneven and less compact protein network structure a large pores and thinner strands was observed in the CH-1 FPI gel, which resulted in a weaker gel strength, as discussed above. However, TS-treated FPI gels had a more uniform microstructure with smaller porosity than CH-1 gels; the microstructure was not significantly different between TS-20 and TS-30 samples, following similar gel strength trends above. The uniform microstructure could be attributed to the production of soluble protein aggregates and β-sheet dominated protein aggregates after TS, which facilities protein-protein interactions and subsequent formation of gel network (Hu, et al., 2013).

3.6.4. Thermo-reversible gelation behaviour of FPI gels

Investigating the rheological behaviour of hydrogels in response to various environmental parameters, such as temperature, is important for their practical application and assists in understanding their underlying gelation mechanism (De Kort, et al., 2016; Yang, Yang, & Yang, 2018). Herein, the temperature responsive rheological property of TS-30 FPI gel was studied, as shown in Fig. 6. When the temperature was increased from 20 to 60 °C, G' and G'' gradually decreased, and G' remained larger than G'', representing a solid-like behaviour. As the temperature increased further from 60 to 80 °C, both G' and G'' decreased significantly, with G' decreasing to a similar value as G''. This indicates a weak gel behaviour with flowability as indicated by the visual appearance shown in Fig. 6 suggesting a gel-sol transition. When the temperature was decreased, both G' and G'' increased, with G' increasing progressively faster than G''. After 75 min, G' was much greater than G'' and the liquid-like sample solidified again to form a hydrogel with a self-supporting behaviour (Fig. 6 inset). Additionally, when the temperature was held at 20 °C for 2 h, G' increased gradually with time, showing that the gel network progressively strengthened. This result suggests that critical role of hydrogen bonding in the formation of TS-induced FPI gel networks (Damodaran, 2008; Yang et al., 2022). Finally, this result demonstrated thermally reversible gelation behaviour of TS-treated FPI at a neutral pH, which may find potential application as a gelatine alternative in vegan food products.

3.7. Physicochemical properties and storage stabilities of emulsions prepared from TS-treated FPI

3.7.1. Oil-water interfacial tension

Fig. 7A illustrates the dependence of interfacial tension (IFT) of FPI dispersions (pH 7) with time before and after TS-30 treatment. An initial significant decrease in the interfacial tension of both samples was observed over time (up to ~1000 s), eventually attaining a plateau at ~6000 s. This indicates that a proportion of the proteins transfer from aqueous phase to the droplet interface (Tang, 2020). The IFT values at 6000 s are shown in Fig. 7A inset and were ~12.35 mN/m (Control) and ~11.51 mN/m (TS-30), respectively, indicating a slightly better interfacial activity of the TS-30 FPI solutions. This may be due to the dominant intermolecular β-sheet structure (Afkhami, Varidi, Varidi, & Hadizadeh, 2023; Lefèvre & Subirade, 2003) and higher surface hydrophobicity (Phoon, San Martin-Gonzalez, & Narsimhan, 2014) of TS-treated FPI as revealed in Fig. 3A and C, which may play an

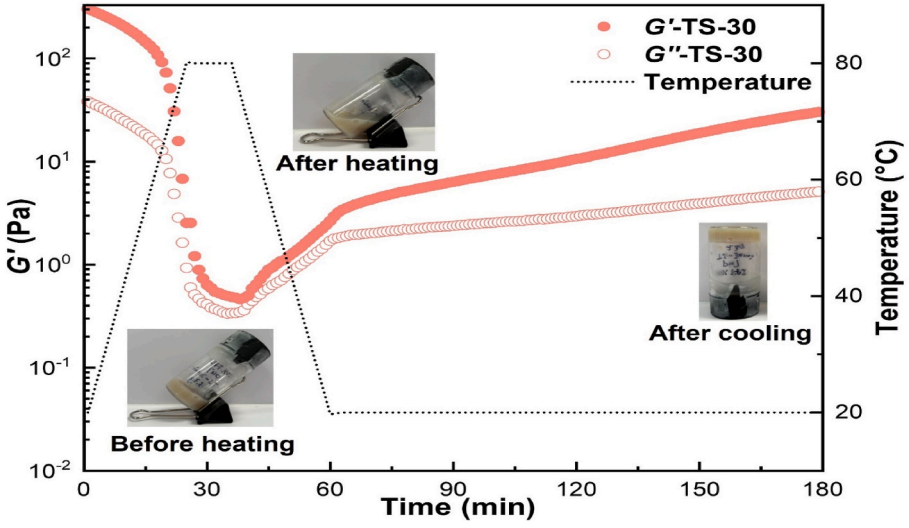

Fig. 6. (A) Storage modulus *G'* (solid symbols) and loss modulus *G''* (empty symbols) as a function of time for faba bean protein isolate (FPI) dispersion (10 wt%, pH 7) treated by thermosonciation for 30 min (TS-30) during a rheological temperature sweep measurement. Inset are visual appearance of samples during sol-gel and gel-sol transitions.

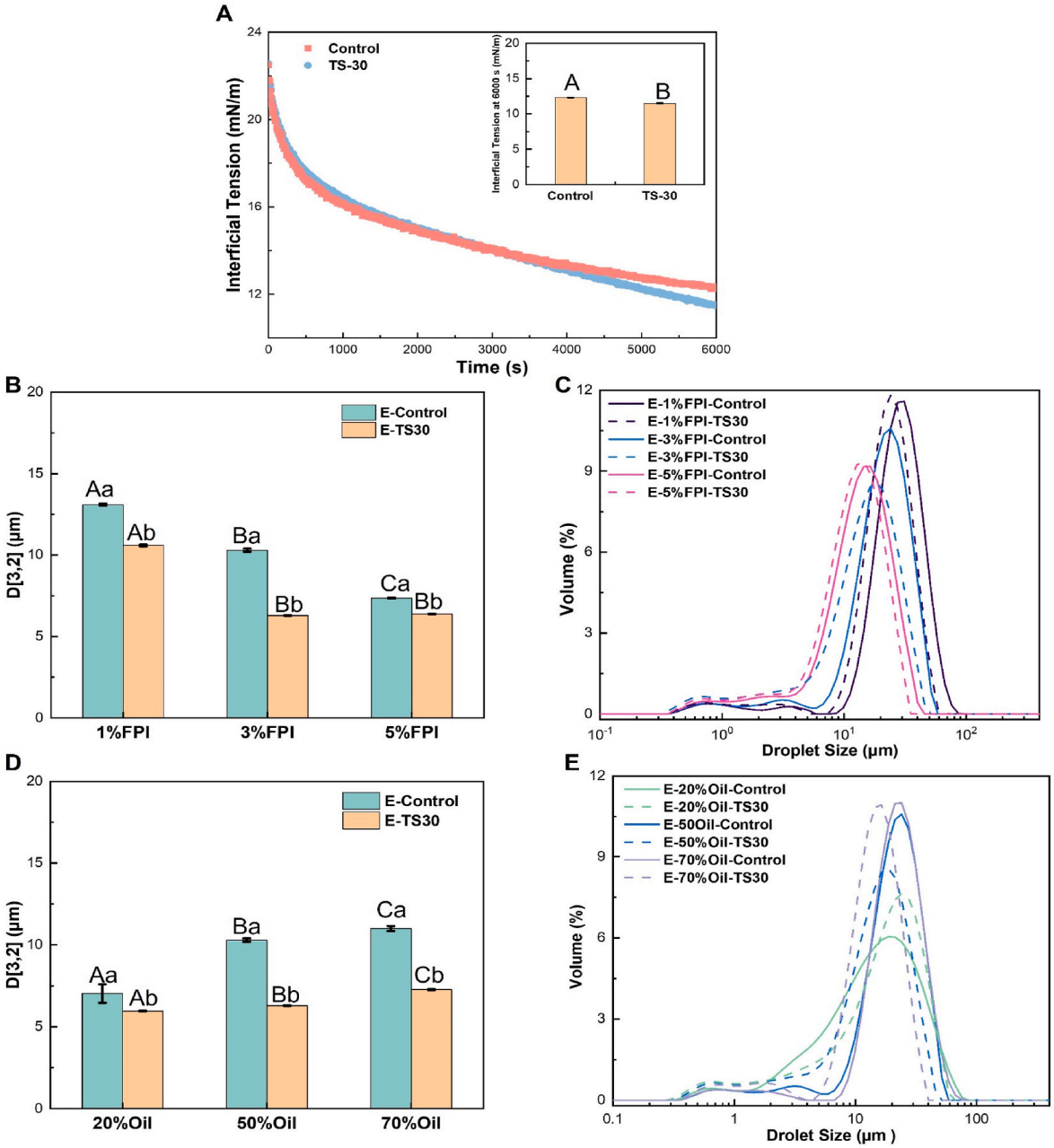

Fig. 7. (A) Time dependence of oil-water interfacial tension of faba bean protein isolate (FPI) before and after 30 min thermosonication treatment (TS-30), and final interfacial tension values at 6000 s (*inset*). (B) Oil droplet size distribution of emulsions stabilised by different concentrations (1, 3, 5 wt%) of native and 30 min thermosonicated FPI (TS-30) at an oil volume fraction of 50% (v/v). (C) Sauter mean diameter D [3,2] of emulsions stabilised by different concentrations (1, 3, 5 wt %) of native and TS-30 treated FPI at oil fraction of 50% (v/v). (D) Sauter mean diameter D [3,2] of emulsion oil droplets stabilised by 3 wt% native or TS-30 treated FPI dispersions at different oil volume fractions (20, 50, and 70%, v/v). (E) Oil droplet size distribution of emulsions stabilised by 3 wt% native or TS-30 treated FPI dispersions at different oil volume fractions (20, 50, and 70%, v/v). In (A) different superscript letters above the column denote significant differences ($P < 0.05$). In (B and D) different capital letters above the columns denote significant differences ($P < 0.05$) in emulsions stabilised by FPI at different concentrations or oil fractions. The different lowercase letters denote significant differences ($P < 0.05$) in emulsions stabilised by FPI solutions with/without TS treatment. E-Control and E-TS30 indicate emulsions stabilised by native FPI and TS-30 treated FPI, respectively.

important role in reducing the oil-water interfacial tension.

3.7.2. Oil droplet size distribution within emulsions

3.7.2.1. Effect of FPI concentrations. The effect of native and TS-treated FPI dispersions on the size distribution is illustrated in Fig. 7B and C. For the native FPI stabilised emulsions, the oil droplet size (D [3,2]) declined from ~13.1 μm to ~7.4 μm as the FPI concentration increasing from 1 wt% to 5 wt% (Fig. 7B). In Fig. 7C, the 1 wt% native FPI stabilised emulsions exhibited a trimodal distribution with a dominant peak at ~40 μm and minor peaks at ~4 μm and ~1 μm, respectively. Increasing the FPI concentration to 5 wt% induce the major peak of the emulsion shifted toward a smaller size to ~12 μm, indicating that the oil droplet size decreases with a rise in FPI concentration. At greater protein concentrations, more proteins are available to cover the newly formed oil surfaces, thus leading to smaller oil droplets (Wynnychuk, et al., 2021; Zhang, Holmes, Ettelaie, & Sarkar, 2020). As shown in Fig. 7B, the oil droplet sizes of the emulsions stabilised by TS-treated FPI were

substantially smaller than the ones stabilised by native FPI at the same protein concentration. Increasing the FPI concentration from 1 to 3 wt% led to a significant decrease in oil droplet sizes from ~10.4 to ~6.3 μm in TS-treated FPI stabilised emulsions. For TS-30 stabilised emulsion, the oil droplet size is similar at ~6.3 μm when FPI concentration increased from 3 wt% to 5 wt%, suggesting that the protein is excess at this oil volume fraction (φ) of 50 %. This discovery is in a good agreement with a study reported by McClements (2004), who found that the oil droplet size is independent of emulsifier concentrations when in excess. In summary, TS-treated FPI is a more effective emulsifier than its native form.

3.7.2.2. Effect of oil volume fraction. The oil droplet size of emulsions stabilised by native or TS-treated FPI is considerably affected by the oil volume fraction φ at a constant protein concentration 3 wt%. When the φ increased from 0.2 to 0.7 in the native FPI prepared emulsions, the oil drop size (D [3,2]) increased from 7.0 to 11.0 μm (Fig. 7D); this is in line with the peak in particle size distribution shifting to a greater value with increasing φ (Fig. 7E). The increase in oil droplet sizes with increasing in φ at constant protein concentrations agrees well with studies on emulsions stabilised by other plant proteins, such as soy protein (Liu & Tang, 2013), lentil protein (Wynnychuk, et al., 2021), and pea protein (Li, Liu, Xu, & Zhang, 2022). The oil droplet sizes of the emulsions stabilised by TS30 were from ~5.9 to ~7.3 μm (Fig. 7D) which were much smaller than the emulsions prepared from native FPI. However, the oil droplet size showed an opposite trend, i.e., the oil droplet size decreases slightly with increasing φ, and the main particle size distribution peak shifted to smaller sizes as shown in Fig. 7D and E. A drop in droplet size with an increase in φ is typically observed when the emulsifiers are in excess. Liu et al. (2013) reported that the oil droplet size of emulsion stabilised by SPI nanoparticles increased with increasing φ from 0.2 to 0.6 at a low SPI concentration (2 wt%) but decreased with increasing φ at a high SPI concentration (6 wt%). When the emulsifier concentration is greater than the interfacial saturation concentration, more proteins were able to adsorb to the droplet surface to enhance the inter-droplet interactions thus leading to the generation of a gel-like network. A high viscosity in the gelled emulsions could impart a high shear stress under turbulent flow during homogenisation thus leading to a more efficient breakup of oil droplets and a decreased droplet size (Tcholakova, et al., 2011). The viscosity of such emulsions is further discussed in **section 3.7.4**.

3.7.3. Microstructure of emulsions

The microstructures of emulsions were also visually observed by light microscopy and CLSM as shown in Fig. 8. Light micrographs showed that the oil droplet size substantially decreased as increasing FPI concentration in emulsions stabilised by native FPI or TS-treated FPI (Fig. 8A). Light micrographs showed that the oil droplet size substantially decreased as increasing FPI concentration in emulsions stabilised by native FPI or TS-treated FPI at a fixed oil volume fraction $\varphi = 0.5$ (Fig. 8A). Furthermore, the oil droplets of emulsions stabilised by TS-30 were substantially smaller than that of the native FPI-stabilised emulsions, consistent with the oil droplet size distribution results. As revealed by CLSM in Fig. 8B, different interfacial layer structures and aqueous phase networks were observed in the native FPI and TS-FPI stabilised emulsions (oil volume fraction $\varphi = 0.5$) at different protein concentrations. In native FPI stabilised emulsions, the proteins formed a thinner interfacial layer on the droplet surfaces and some protein aggregates were observed in the aqueous phase. However, TS-30 stabilised emulsions had a thicker interfacial layer on the droplet surfaces and some localized gel-networks can be observed due to bridging between adjacent droplets, in particular in emulsions with high protein concentrations of 3 and 5 wt% TS-FPI. The droplet networking was also evident in the tube inversion test as shown in Fig. S1, where emulsions do not flow upon inverted. This could be due to the interactions and entanglements between protein aggregates in the aqueous phase and/or bridging of oil droplets, leading to the formation of a gel network structure (Bai, Huan, Xiang, & Rojas, 2018; Tang & Ghosh, 2021).

The microstructures of emulsions with different φ at a fixed 3 wt %

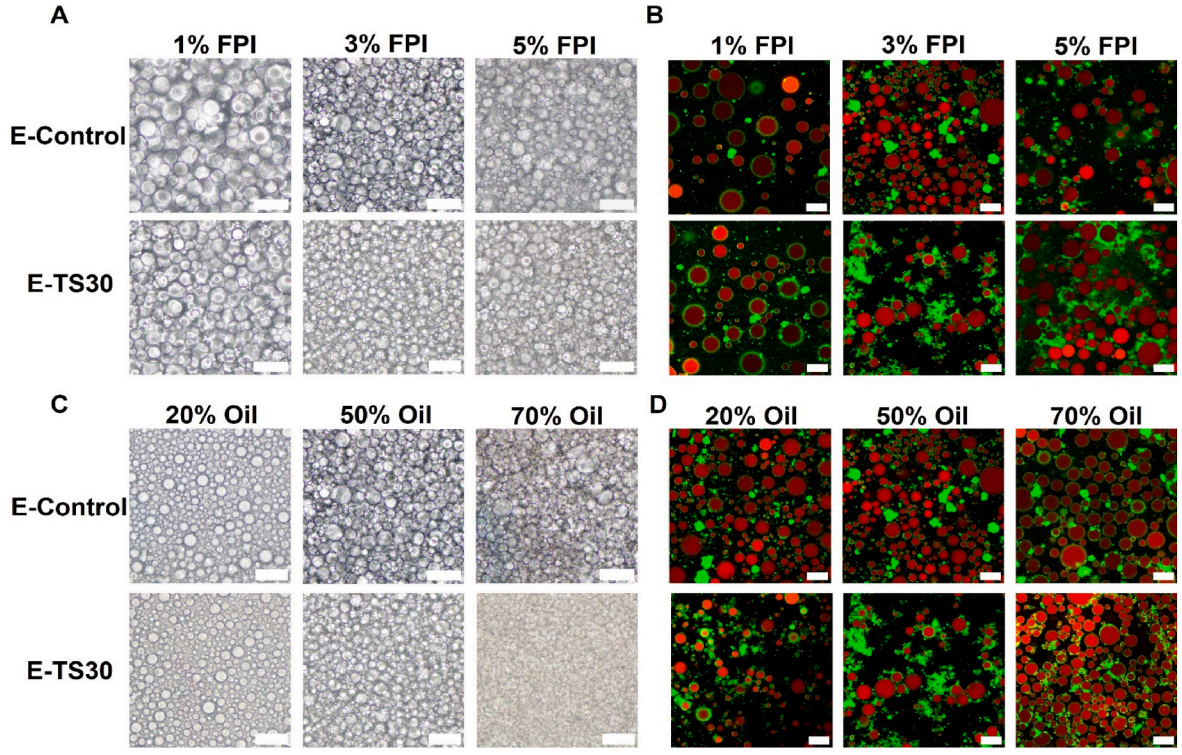

Fig. 8. Optical microscopic (left) and confocal laser scanning microscopic (CLSM) (right) images of (A and B) emulsions stabilised by different concentrations (1, 3, 5 wt%) of native and TS-30 treated faba bean protein isolate (FPI) dispersions at an oil volume fraction of 50% (v/v). Optical microscopic images (C) and CLSM images (D) of emulsion stabilised by 3 wt% native and TS-30 treated FPI dispersions at different oil volume fractions (20, 50, and 70%, v/v). Scale bar = 20 μm.

FPI concentration were also investigated (Fig. 8C and D). It can be seen that the oil droplet packing became denser with increasing φ in the emulsion stabilised by 3 wt% native and TS-treated FPI (Fig. 8C) (Liu et al., 2013). The oil droplet size of emulsion stabilised by native FPI was increased with increasing oil fraction. In addition, droplet flocculation became more visible with increasing oil fraction (Fig. 8D), in particular at oil volume fraction $\varphi = 0.7$, which gave rise to emulsion gel network formation as also observed in Fig. S1. The gel-like network with a high oil fraction has also been reported in the emulsions stabilised by other plant proteins, such as SPI (Tang & Liu, 2013), FPI (Hu, et al., 2023), and pea protein (Velez-Erazo, Bosqui, Rabelo, Kurozawa, & Hubinger, 2020). In emulsions stabilised by TS-treated FPI, oil droplet sizes decreased with increasing φ (Fig. 8C), which agreed well with particle sizing results (Fig. 7E). Further, CLSM revealed that the oil droplets stabilised by TS-treated FPI have a thicker interfacial layer and greater network formation due to protein aggregate entanglement and droplet-droplet interactions compared to the emulsions stabilised by native FPI. The microstructural differences could result in differences in mechanical properties, which will be discussed in the following section.

3.7.4. Rheological properties of emulsions

3.7.4.1. Small deformation rheological properties of emulsions. The viscoelastic response of emulsion systems stabilised by native or TS-treated FPI as a function of frequency is illustrated in Fig. 9 A to D. G' and G'' of all the samples were parallel to each other with a slight dependence on frequency, indicating that all samples were dominated by an elastic behaviour consistent with a gel (Banerjee et al., 2012). The emulsion systems stabilised by native FPI were found to be weaker, which was also confirmed by previous findings. The greater gel strength found in TS-30 FPI stabilised emulsions could be attributed to interactions and entanglements of FPI protein aggregates located on the oil-water interface of neighbouring small oil droplets, compact arrangement of oil droplets, and thick interfacial layer of FPI aggregates as revealed by CLSM (Fig. 8) (Hu, et al., 2023; Kornet et al., 2022).

The G' (1 Hz) of all emulsions stabilised by various FPI concentrations is plotted in Fig. 9E. An increase in the FPI concentration resulted in the increased gel strength of the emulsions. Specifically, in native FPI stabilised emulsions, G' (1 Hz) increased from ~1 Pa for 1 wt% FPI stabilised emulsion to ~18 Pa for 5 wt% FPI stabilised emulsion. While for TS-30 FPI stabilised emulsion, G' (1 Hz) increased dramatically from ~8 Pa (1 wt% FPI) to ~250 Pa (5 wt% FPI). This finding is consistent with reports on other plant protein (e.g. QPI) stabilised emulsions (Hu, et al., 2023; Zhang, Cheng, Luo, Hemar, & Yang, 2021). The stronger gel found at higher FPI concentrations could be due to the smaller oil droplet size, compact interactions between adjacent oil droplets and protein network formation in the continuous phase as revealed by CLSM in Fig. 8.

The effect of oil volume faction on the gel strength G' (1 Hz) of native/TS-treated FPI stabilised emulsions is shown in Fig. 9F. Similar to Fig. 9E, emulsions prepared by TS-treated FPI exhibited significantly higher G' values ranging from ~6 Pa to ~1121 Pa with increasing oil fraction φ from 0.2 to 0.7 compared to native FPI (~0.53 Pa to ~662 Pa). Additionally, it can be assumed that the greater the oil fraction, the greater the gel strength. At continuously increasing oil fractions, the number of dispersed oil droplets will increase, leading to a higher packing state of the droplets (Brinkman, 1952). The number of interactions between protein particles and oil droplets also increases, thus leading to the increase in gel strength at higher oil ratios (Krieger & Dougherty, 1959).

3.7.4.2. Large deformation rheological properties of emulsions. The strain dependent rheological characteristics of emulsions are shown in Fig. 10. G' and G'' of all the samples were independent of strain amplitude within the LVR, with G' being larger than G'', which confirmed the gel-like network structure of all emulsion systems as shown in Fig. 9 (Zou, Yang, & Scholten, 2018). Once the strain amplitude was above the LVR, the G' values for all samples decreased substantially, indicating structural disintegration. For emulsions stabilised by TS-treated FPI, the G'' values increased with strain amplitude and reached a local maximum, which has been assigned as type III nonlinear (weak strain overshoot) behaviour (Hyun, et al., 2002). This could have resulted from structural rearrangements under large strain deformation (Masalova, Foudazi, & Malkin, 2011; Mason, Bibette, & Weitz, 1995; Zhang, Cheng, et al., 2021). For most native FPI-stabilised samples, Type I (*strain thinning*) behaviour was observed (Fig. 10) as G' and G'' decreased monotonically with increasing strain (Hyun, et al., 2002; Zhang, Lu, Zhang, Gao, & Mao, 2021). Xu et al. (2023) attributed this Type I behaviour to the rearrangement of the emulsion microstructure with the direction of flow field.

The values of breaking stress (σ_b) are shown in Fig. 10C and F. In line with the small deformation rheology results, the σ_b values of emulsions stabilised by TS-treated FPI were significantly greater than those of native FPI stabilised emulsions. Specifically, as the untreated FPI concentration rise from 1 to 5 wt%, the σ_b slightly increased from ~0.4–~7 Pa, whereas TS-30 stabilised emulsion had a larger σ_b in the range of ~0.7–~38 Pa, indicating a stronger gel was formed. Also, σ_b increased with an increase in oil fraction, which agrees well with the small deformation rheological findings.

3.7.5. Long-term storage stability of emulsions

Fig. S1 shows photographs of emulsions stabilised by native or TS-30-treated FPI (1, 3 and 5 wt%) containing oil volume fractions of 0.2, 0.5, and 0.7 over a storage period of 28 days at 20 °C. Fig. S2 shows the creaming index and volume-weighted mean droplet diameter (D [4,3]) of the emulsions during storage. In all samples, a cream layer and high serum phase were clearly observed along with an increase in creaming index and D [4,3] of oil droplets increasing with storage time (Figs. S2A and B). In addition, as the FPI concentration increased, the creaming phenomenon and oil droplet coalescence decreased. Furthermore, emulsions containing higher oil fractions also exhibited superior stabilities, which could be due to gel network formation as revealed by rheology and CLSM observations (McClements, 2007). Finally, at all conditions, emulsions stabilised by TS-30 FPI showed greater stability compared to the emulsions stabilised by native FPI. This could be explained by the smaller oil droplet size, denser and more compact arrangement of oil droplets (especially at a high oil volume fraction), and greater mechanical strength found in emulsions stabilised by TS-30 FPI. In general, this study suggested that TS treatment is promising and efficient to enhance emulsification capability and stability of FPI for use in emulsion-based beverage and gels.

4. Conclusions

This study systematically studied the impacts of thermosonication (TS) on the physicochemical properties, techno-functional performances, and microstructural characteristics of FPI dispersions at pH 7 and compared with the conventional heating (CH) method. The results demonstrated that the TS treatment formed FPI protein aggregates that are rich in β-sheet secondary structures, as evidenced by ThT fluorescence, CD spectra, TEM, and SANS results. This may be due to extensive denaturation and unfolding of FPI molecules when exposed to ultrasonication at high temperatures followed by structural rearrangements and assembly. In addition, TS significantly decreased FPI particle size and increased the solubility. The formation of a thermoreversible viscoelastic gel network was identified in TS-induced 10 wt% FPI dispersions, suggesting potential applications as a texturizer in vegan food products. Finally, different concentrations of TS-30 treated FPI dispersions (1, 3, and 5 wt%) were used to stabilise O/W emulsions at various oil volume fractions ($\varphi = 0.2$, 0.5, and 0.7). The emulsions formed by TS-30 treated FPI exhibited smaller oil droplet size, greater mechanical

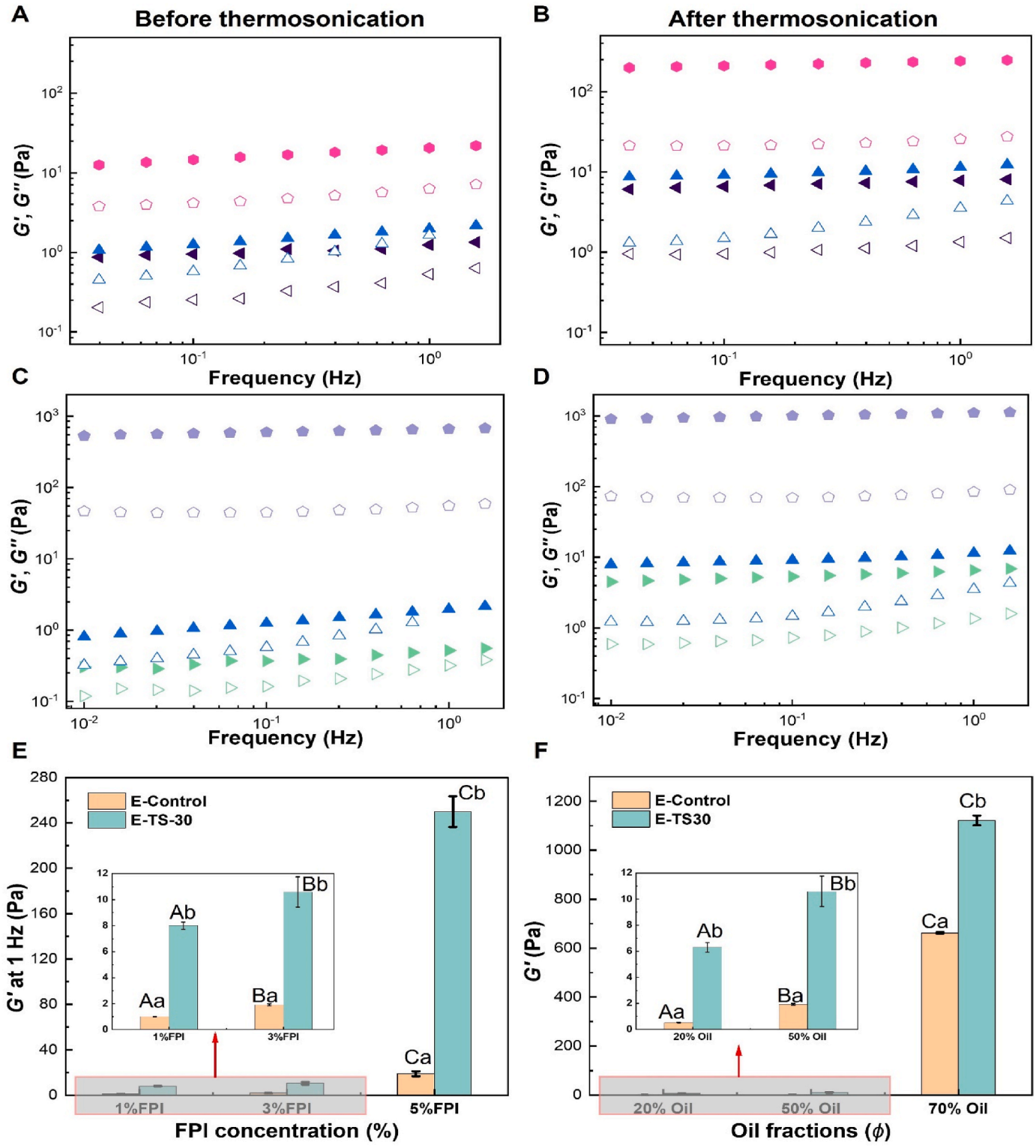

Fig. 9. The frequency dependence of G' (solid symbols) and G'' (empty symbols) for emulsions stabilised by faba bean protein isolate (FPI) before (A and C) and after (B and D) 30 min thermosinication treatment (TS-30). (A and B) Emulsions stabilised by different concentrations of native and TS-30 treated FPI dispersion (1, 3, 5 wt %) at an oil volume fraction of 50% (v/v). Symbols correspond to: 1 wt% FPI (◀), 3 wt% FPI (▲), and 5 wt% FPI (⬢). (C and D) Emulsions stabilised by 3 wt% native and TS-30 treated FPI dispersion at different oil fractions (20, 50, and 70%, v/v). Symbols correspond to: 20% oil (▶), 50% oil (▲), and 70% oil (⬟). (E and F) G' (1 Hz) of emulsions stabilised by untreated and TS-30 treated FPI. Different superscript capital letters above columns denote significant differences ($P < 0.05$) between the emulsions stabilised by different concentrations of FPI (1, 3, 5 wt%) or different oil volume fractions (20, 50, and 70%, v/v). Above the column, different lowercase superscripts denote significant differences ($P < 0.05$) between the emulsion systems prepared by FPI treated with/without TS.

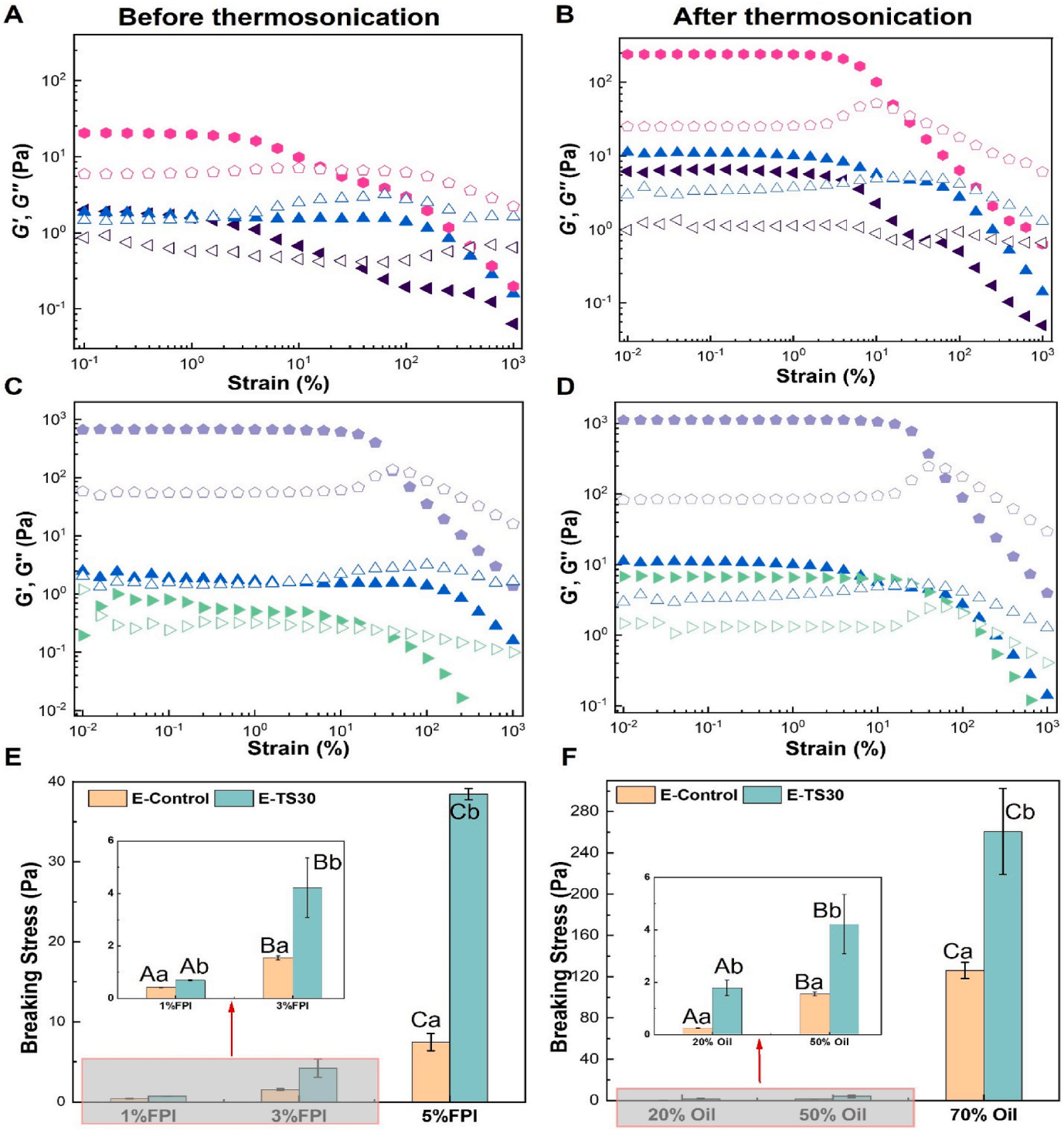

Fig. 10. The G' (solid symbols) and G'' (empty symbols) as a function of strain amplitude for emulsions stablised by faba bean protein isolate (FPI) before (A and C) and after (B and D) thermosinication treatment for 30 min (TS-30). (A and B) Emulsions stabilised by different concentrations of native and TS-30 treated FPI dispersion (1, 3, 5 wt%) at an oil volume fraction of 50% (v/v). Symbols correspond to: 1 wt% FPI (◀), 3 wt% FPI (▲), and 5 wt% FPI (⬢). (C and D) Emulsions stabilised by 3 wt% native and TS-30 treated FPI dispersion at different oil fractions (20, 50, and 70%, v/v). Symbols correspond to: 20% oil (▶), 50% oil (▲), and 70% oil (⬟). (E and F) Breaking stress of all emulsion systems. Different superscript capital letters above columns denote significant differences ($P < 0.05$) between the emulsions stabilised by different concentrations of FPI (1, 3, 5 wt%) or different oil volume fractions (20, 50, and 70%, v/v). The different lowercase letters denote significant differences ($P < 0.05$) between the emulsion systems stabilised by FPI treated with/without TS.

strength, more compact and denser oil droplet microstructure, as well as a better storage stability than those formed by the native FPI. In summary, this study showed that the TS treatment can form FPI protein aggregates at pH 7 with distinctive gelation behaviour and improved emulsification capability. The resulting new structures of FPI offers a range of potential applications for use as a texturing and emulsifying agent in food, cosmetic, and pharmaceutical products.

CRediT authorship contribution statement

Yinxuan Hu: Writing – original draft, Visualization, Methodology, Investigation. **Lirong Cheng:** Writing – review & editing, Validation, Supervision, Formal analysis, Data curation, Conceptualization. **Elliot Paul Gilbert:** Writing – review & editing, Visualization, Validation, Resources, Methodology, Investigation, Formal analysis, Data curation. **Sung Je Lee:** Writing – review & editing, Validation, Supervision. **Zhi Yang:** Writing – original draft, Writing – review & editing, Supervision, Resources, Project administration, Methodology, Funding acquisition, Formal analysis, Data curation, Conceptualization.

Declaration of competing interest

The authors declare that they do not have conflict of interest.

Data availability

Data will be made available on request.

Acknowledgements

The author Yinxuan Hu would like to thank Massey University, New Zealand, for providing a doctoral scholarship. We thank the Manawatu Microscopy and Imaging Centre (MMIC) at Massey University, Palmerston North for their kind support and assistance. The authors thank the support of the Australian Centre for Neutron Scattering, ANSTO in supporting the QUOKKA neutron research infrastructure used in this work via ACNS proposal P15802.

Appendix A. Supplementary data

Supplementary data to this article can be found online at https://doi.org/10.1016/j.foodhyd.2024.110140.

References

Afkhami, R., Varidi, M. J., Varidi, M., & Hadizadeh, F. (2023). Boosting emulsion properties: The role of β-sheet content and fibril length in soy protein isolate emulsions. *Food Hydrocolloids*, Article 109513.

Akharume, F. U., Aluko, R. E., & Adedeji, A. A. (2021). Modification of plant proteins for improved functionality: A review. *Comprehensive Reviews in Food Science and Food Safety, 20*(1), 198–224.

Alavi, F., Chen, L., & Emam-Djomeh, Z. (2021). Effect of ultrasound-assisted alkaline treatment on functional property modifications of faba bean protein. *Food Chemistry, 354*, Article 129494.

Alavi, F., Chen, L., Wang, Z., & Emam-Djomeh, Z. (2021). Consequences of heating under alkaline pH alone or in the presence of maltodextrin on solubility, emulsifying and foaming properties of faba bean protein. *Food Hydrocolloids, 112*, Article 106335.

Armelin, E., Martí, M., Rudé, E., Labanda, J., Llorens, J., & Alemán, C. (2006). A simple model to describe the thixotropic behavior of paints. *Progress in Organic Coatings, 57*(3), 229–235.

Augustin, M., & Cole, M. (2022). Towards a sustainable food system by design using faba bean protein as an example. *Trends in Food Science & Technology, 125*, 1–11.

Bai, L., Huan, S., Xiang, W., & Rojas, O. J. (2018). Pickering emulsions by combining cellulose nanofibrils and nanocrystals: Phase behavior and depletion stabilization. *Green Chemistry, 20*(7), 1571–1582.

Banc, A., Charbonneau, C., Dahesh, M., Appavou, M.-S., Fu, Z., Morel, M.-H., et al. (2016). Small angle neutron scattering contrast variation reveals heterogeneities of interactions in protein gels. *Soft Matter, 12*(24), 5340–5352.

Banerjee, S., & Bhattacharya, S. (2012). Food gels: Gelling process and new applications. *Critical Reviews in Food Science and Nutrition, 52*(4), 334–346.

Beck, S. M., Knoerzer, K., Sellahewa, J., Emin, M. A., & Arcot, J. (2017). Effect of different heat-treatment times and applied shear on secondary structure, molecular weight distribution, solubility and rheological properties of pea protein isolate as investigated by capillary rheometry. *Journal of Food Engineering, 208*, 66–76.

Biancalana, M., & Koide, S. (2010). Molecular mechanism of Thioflavin-T binding to amyloid fibrils. *Biochimica et Biophysica Acta (BBA)-Proteins and Proteomics, 1804*(7), 1405–1412.

Boukari, H., Lin, J., & Harris, M. (1997). Small-angle X-ray scattering study of the formation of colloidal silica particles from alkoxides: Primary particles or not? *Journal of Colloid and Interface Science, 194*(2), 311–318.

Brinkman, H. C. (1952). The viscosity of concentrated suspensions and solutions. *The Journal of Chemical Physics, 20*(4), 571-571.

Chen, L., Ettelaie, R., & Akhtar, M. (2019). Improved enzymatic accessibility of peanut protein isolate pre-treated using thermosonication. *Food Hydrocolloids, 93*, 308–316.

Cheng, L., Ye, A., Yang, Z., Gilbert, E. P., Knott, R., de Campo, L., et al. (2022). Small-angle X-ray scattering (SAXS) and small-angle neutron scattering (SANS) study on the structure of sodium caseinate in dispersions and at the oil-water interface: Effect of calcium ions. *Food Structure, 32*, Article 100276.

da Silva, A. M. M., Almeida, F. S., & Sato, A. C. K. (2021). Functional characterization of commercial plant proteins and their application on stabilization of emulsions. *Journal of Food Engineering, 292*, Article 110277.

Damodaran, S. (2008). Amino acids, peptides and proteins. *Fennema's Food Chemistry, 4*, 425–439.

De Kort, D. W., Veen, S. J., Van As, H., Bonn, D., Velikov, K. P., & Van Duynhoven, J. P. (2016). Yielding and flow of cellulose microfibril dispersions in the presence of a charged polymer. *Soft Matter, 12*(21), 4739–4744.

Du, H., Lin, Y., Stanton, C., Daniloski, D., Zannini, E., Ross, R. P., et al. (2023). Characterization and functional properties of pH-and heated time-induced aggregates from red lentil protein. *Food Structure, 37*, Article 100342.

Fang, Z., Cai, X., Wu, J., Zhang, L., Fang, Y., & Wang, S. (2021). Effect of simultaneous treatment combining ultrasonication and pH-shifting on SPI in the formation of nanoparticles and encapsulating resveratrol. *Food Hydrocolloids, 111*, Article 106250.

Fasman, G. D. (2013). *Circular dichroism and the conformational analysis of biomolecules*. Springer Science & Business Media.

Frydenberg, R. P., Hammershøj, M., Andersen, U., Greve, M. T., & Wiking, L. (2016). Protein denaturation of whey protein isolates (WPIs) induced by high intensity ultrasound during heat gelation. *Food Chemistry, 192*, 415–423.

Gilbert, E. P., Schulz, J. C., & Noakes, T. J. (2006). 'Quokka'—the small-angle neutron scattering instrument at OPAL. *Physica B: Condensed Matter, 385*, 1180–1182.

Goeden-Wood, N. L., Keasling, J. D., & Muller, S. J. (2003). Self-assembly of a designed protein polymer into β-sheet fibrils and responsive gels. *Macromolecules, 36*(8), 2932–2938.

Greenfield, N. J. (2006). Using circular dichroism spectra to estimate protein secondary structure. *Nature Protocols, 1*(6), 2876–2890.

Grossmann, L., & McClements, D. J. (2023). Current insights into protein solubility: A review of its importance for alternative proteins. *Food Hydrocolloids, 137*, Article 108416.

Guimarães, J. T., Silva, E. K., Alvarenga, V. O., Costa, A. L. R., Cunha, R. L., Sant'Ana, A. S., et al. (2018). Physicochemical changes and microbial inactivation after high-intensity ultrasound processing of prebiotic whey beverage applying different ultrasonic power levels. *Ultrasonics Sonochemistry, 44*, 251–260.

Gülseren, İ., Güzey, D., Bruce, B. D., & Weiss, J. (2007). Structural and functional changes in ultrasonicated bovine serum albumin solutions. *Ultrasonics Sonochemistry, 14*(2), 173–183.

Guo, F., Xiong, Y. L., Qin, F., Jian, H., Huang, X., & Chen, J. (2015). Surface properties of heat-induced soluble soy protein aggregates of different molecular masses. *Journal of Food Science, 80*(2), C279–C287.

Hammouda, B., Ho, D. L., & Kline, S. (2004). Insight into clustering in poly (ethylene oxide) solutions. *Macromolecules, 37*(18), 6932–6937.

Herneke, A., Lendel, C., Johansson, D., Newson, W., Hedenqvist, M., Karkehabadi, S., et al. (2021). Protein nanofibrils for sustainable food–characterization and comparison of fibrils from a broad range of plant protein isolates. *ACS Food Science & Technology, 1*(5), 854–864.

Hernoux Villière, A., Lassi, U., & Lévêque, J. M. (2013). An original ultrasonic reaction with dual coaxial frequencies for biomass processing. *Ultrasonics Sonochemistry, 20*(6), 1341–1344.

Hu, Y., Cheng, L., Lee, S. J., & Yang, Z. (2023). Formation and characterisation of concentrated emulsion gels stabilised by faba bean protein isolate and its applications for 3D food printing. *Colloids and Surfaces A: Physicochemical and Engineering Aspects*, Article 131622.

Hu, H., Li-Chan, E. C., Wan, L., Tian, M., & Pan, S. (2013). The effect of high intensity ultrasonic pre-treatment on the properties of soybean protein isolate gel induced by calcium sulfate. *Food Hydrocolloids, 32*(2), 303–311.

Hyun, K., Kim, S. H., Ahn, K. H., & Lee, S. J. (2002). Large amplitude oscillatory shear as a way to classify the complex fluids. *Journal of Non-newtonian Fluid Mechanics, 107*(1–3), 51–65.

Jiang, S., Ding, J., Andrade, J., Rababah, T. M., Almajwal, A., Abulmeaty, M. M., et al. (2017). Modifying the physicochemical properties of pea protein by pH-shifting and ultrasound combined treatments. *Ultrasonics Sonochemistry, 38*, 835–842.

Jiang, J., Wang, Q., & Xiong, Y. L. (2018). A pH shift approach to the improvement of interfacial properties of plant seed proteins. *Current Opinion in Food Science, 19*, 50–56.

Jo, Y.-J., Huang, W., & Chen, L. (2020). Fabrication and characterization of lentil protein gels from fibrillar aggregates and the gelling mechanism study. *Food & Function, 11*(11), 10114–10125.

Josefsson, L., Ye, X., Brett, C. J., Meijer, J., Olsson, C., Sjögren, A., et al. (2019). Potato protein nanofibrils produced from a starch industry sidestream. *ACS Sustainable Chemistry & Engineering, 8*(2), 1058–1067.

Karolkowski, A., Martin, C., Bouzidi, E., Albouy, J.-F., Levavasseur, L., Briand, L., et al. (2022). Heat treatment, cultivar and formulation modify the sensory properties and consumer acceptability of gels containing faba bean (Vicia faba L. minor) protein concentrates. *Foods, 11*(19), 3018.

Kaspchak, E., de Oliveira, M. A. S., Simas, F. F., Franco, C. R. C., Silveira, J. L. M., Mafra, M. R., et al. (2017). Determination of heat-set gelation capacity of a quinoa protein isolate (Chenopodium quinoa) by dynamic oscillatory rheological analysis. *Food Chemistry, 232*, 263–271.

Kato, A., & Nakai, S. (1980). Hydrophobicity determined by a fluorescence probe method and its correlation with surface properties of proteins. *Biochimica et Biophysica Acta (BBA) - Protein Structure, 624*(1), 13–20.
Khatkar, A. B., Kaur, A., & Khatkar, S. K. (2020). Restructuring of soy protein employing ultrasound: Effect on hydration, gelation, thermal, in-vitro protein digestibility and structural attributes. *LWT, 132*, Article 109781.
Kline, S. R. (2006). Reduction and analysis of SANS and USANS data using IGOR Pro. *Journal of Applied Crystallography, 39*(6), 895–900.
Kong, J., & Yu, S. (2007). Fourier transform infrared spectroscopic analysis of protein secondary structures. *Acta Biochimica et Biophysica Sinica, 39*(8), 549–559.
Kornet, R., Sridharan, S., Venema, P., Sagis, L. M., Nikiforidis, C. V., van der Goot, A. J., et al. (2022). Fractionation methods affect the gelling properties of pea proteins in emulsion-filled gels. *Food Hydrocolloids, 125*, Article 107427.
Krieger, I. M., & Dougherty, T. J. (1959). A mechanism for non-Newtonian flow in suspensions of rigid spheres. *Transactions of the Society of Rheology, 3*(1), 137–152.
Kutzli, I., Zhou, J., Li, T., Baier, S. K., & Mezzenga, R. (2023). Formation and characterization of plant-based amyloid fibrils from hemp seed protein. *Food Hydrocolloids, 137*, Article 108307.
Langton, M., Ehsanzamir, S., Karkehabadi, S., Feng, X., Johansson, M., & Johansson, D. P. (2020). Gelation of faba bean proteins-Effect of extraction method, pH and NaCl. *Food Hydrocolloids, 103*, Article 105622.
Lefevre, T., & Subirade, M. (2000). Molecular differences in the formation and structure of fine-stranded and particulate β-lactoglobulin gels. *Biopolymers: Original Research on Biomolecules, 54*(7), 578–586.
Lefèvre, T., & Subirade, M. (2003). Formation of intermolecular β-sheet structures: A phenomenon relevant to protein film structure at oil–water interfaces of emulsions. *Journal of Colloid and Interface Science, 263*(1), 59–67.
Li, X. L., Liu, W. J., Xu, B. C., & Zhang, B. (2022). Simple method for fabrication of high internal phase emulsions solely using novel pea protein isolate nanoparticles: Stability of ionic strength and temperature. *Food Chemistry, 370*, Article 130899.
Liu, F., & Tang, C.-H. (2013). Soy protein nanoparticle aggregates as pickering stabilizers for oil-in-water emulsions. *Journal of Agricultural and Food Chemistry, 61*(37), 8888–8898.
Loveday, S. M. (2019). Food proteins: Technological, nutritional, and sustainability attributes of traditional and emerging proteins. *Annual Review of Food Science and Technology, 10*, 311–339.
Luo, L., Cheng, L., Zhang, R., & Yang, Z. (2022). Impact of high-pressure homogenization on physico-chemical, structural, and rheological properties of quinoa protein isolates. *Food Structure, 32*, Article 100265.
Luo, L., Yang, Z., Wang, H., Ashokkumar, M., & Hemar, Y. (2022). Impacts of sonication and high hydrostatic pressure on the structural and physicochemical properties of quinoa protein isolate dispersions at acidic, neutral and alkaline pHs. *Ultrasonics Sonochemistry, 91*, Article 106232.
Luo, L., Zhang, R., Palmer, J., Hemar, Y., & Yang, Z. (2021). Impact of high hydrostatic pressure on the gelation behavior and microstructure of quinoa protein isolate dispersions. *ACS Food Science & Technology, 1*(11), 2144–2151.
Martínez-Velasco, A., Lobato-Calleros, C., Hernández-Rodríguez, B. E., Román-Guerrero, A., Alvarez-Ramirez, J., & Vernon-Carter, E. J. (2018). High intensity ultrasound treatment of faba bean (Vicia faba L.) protein: Effect on surface properties, foaming ability and structural changes. *Ultrasonics Sonochemistry, 44*, 97–105.
Masalova, I., Foudazi, R., & Malkin, A. Y. (2011). The rheology of highly concentrated emulsions stabilized with different surfactants. *Colloids and Surfaces A: Physicochemical and Engineering Aspects, 375*(1–3), 76–86.
Mason, T., Bibette, J., & Weitz, D. (1995). Elasticity of compressed emulsions. *Physical Review Letters, 75*(10), 2051.
McCarthy, N. A., Kennedy, D., Hogan, S. A., Kelly, P. M., Thapa, K., Murphy, K. M., et al. (2016). Emulsification properties of pea protein isolate using homogenization, microfluidization and ultrasonication. *Food Research International, 89*, 415–421.
McClements, D. J. (2004). Protein-stabilized emulsions. *Current Opinion in Colloid & Interface Science, 9*(5), 305–313.
McClements, D. J. (2007). Critical review of techniques and methodologies for characterization of emulsion stability. *Critical Reviews in Food Science and Nutrition, 47*(7), 611–649.
Monteiro, S. H., Silva, E. K., Alvarenga, V. O., Moraes, J., Freitas, M. Q., Silva, M. C., et al. (2018). Effects of ultrasound energy density on the non-thermal pasteurization of chocolate milk beverage. *Ultrasonics Sonochemistry, 42*, 1–10.
Munialo, C. D., Martin, A. H., Van Der Linden, E., & De Jongh, H. H. (2014). Fibril formation from pea protein and subsequent gel formation. *Journal of Agricultural and Food Chemistry, 62*(11), 2418–2427.
Napieraj, M., Brûlet, A., Lutton, E., Randrianarisoa, U., Boire, A., & Boué, F. (2022). Monitoring food structure in plant protein gels during digestion: Rheometry and Small Angle Neutron Scattering studies. *Food Structure, 32*, Article 100270.
Ningtyas, D. W., Tam, B., Bhandari, B., & Prakash, S. (2021). Effect of different types and concentrations of fat on the physico-chemical properties of soy protein isolate gel. *Food Hydrocolloids, 111*, Article 106226.
Nivala, O., Mäkinen, O. E., Kruus, K., Nordlund, E., & Ercili-Cura, D. (2017). Structuring colloidal oat and faba bean protein particles via enzymatic modification. *Food Chemistry, 231*, 87–95.
Nivala, O., Nordlund, E., Kruus, K., & Ercili-Cura, D. (2021). The effect of heat and transglutaminase treatment on emulsifying and gelling properties of faba bean protein isolate. *LWT, 139*, Article 110517.
Ó Flynn, T. D., Hogan, S. A., Daly, D. F., Ó Mahony, J. A., & McCarthy, N. A. (2021). Rheological and solubility properties of soy protein isolate. *Molecules, 26*(10), 3015.
Phoon, P. Y., San Martin-Gonzalez, M. F., & Narsimhan, G. (2014). Effect of hydrolysis of soy β-conglycinin on the oxidative stability of O/W emulsions. *Food Hydrocolloids, 35*, 429–443.
Samaei, S. P., Ghorbani, M., Tagliazucchi, D., Martini, S., Gotti, R., Themelis, T., et al. (2020). Functional, nutritional, antioxidant, sensory properties and comparative peptidomic profile of faba bean (Vicia faba, L.) seed protein hydrolysates and fortified apple juice. *Food Chemistry, 330*, Article 127120.
Schwenke, K. (2001). Reflections about the functional potential of legume proteins A Review. *Food, 45*(6), 377–381.
Speroni, F., Beaumal, V., de Lamballerie, M., Anton, M., Añón, M., & Puppo, M. (2009). Gelation of soybean proteins induced by sequential high-pressure and thermal treatments. *Food Hydrocolloids, 23*(5), 1433–1442.
Sponton, O. E., Perez, A. A., Ramel, J. V., & Santiago, L. G. (2017). Protein nanovehicles produced from egg white. Part 1: Effect of pH and heat treatment time on particle size and binding capacity. *Food Hydrocolloids, 73*, 67–73.
Stathopulos, P. B., Scholz, G. A., Hwang, Y. M., Rumfeldt, J. A., Lepock, J. R., & Meiering, E. M. (2004). Sonication of proteins causes formation of aggregates that resemble amyloid. *Protein Science, 13*(11), 3017–3027.
Taha, A., Hu, T., Zhang, Z., Bakry, A. M., Khalifa, I., Pan, S., et al. (2018). Effect of different oils and ultrasound emulsification conditions on the physicochemical properties of emulsions stabilized by soy protein isolate. *Ultrasonics Sonochemistry, 49*, 283–293.
Tamang, N., Shrestha, P., Khadka, B., Mondal, M. H., Saha, B., & Bhattarai, A. (2021). A review of biopolymers' utility as emulsion stabilizers. *Polymers, 14*(1), 127.
Tang, C. (2020). Globular proteins as soft particles for stabilizing emulsions: Concepts and strategies. *Food Hydrocolloids, 103*, Article 105664.
Tang, Y. R., & Ghosh, S. (2021). Stability and rheology of canola protein isolate-stabilized concentrated oil-in-water emulsions. *Food Hydrocolloids, 113*, Article 106399.
Tang, C., & Liu, F. (2013). Cold, gel-like soy protein emulsions by microfluidization: Emulsion characteristics, rheological and microstructural properties, and gelling mechanism. *Food Hydrocolloids, 30*(1), 61–72.
Tang, C., Wang, S., & Huang, Q. (2012). Improvement of heat-induced fibril assembly of soy β-conglycinin (7S Globulins) at pH 2.0 through electrostatic screening. *Food Research International, 46*(1), 229–236.
Tcholakova, S., Lesov, I., Golemanov, K., Denkov, N. D., Judat, S., Engel, R., et al. (2011). Efficient emulsification of viscous oils at high drop volume fraction. *Langmuir, 27*(24), 14783–14796.
Velez-Erazo, E. M., Bosqui, K., Rabelo, R. S., Kurozawa, L. E., & Hubinger, M. D. (2020). High internal phase emulsions (HIPE) using pea protein and different polysaccharides as stabilizers. *Food Hydrocolloids, 105*, Article 105775.
Villamiel, M., & de Jong, P. (2000). Influence of high-intensity ultrasound and heat treatment in continuous flow on fat, proteins, and native enzymes of milk. *Journal of Agricultural and Food Chemistry, 48*(2), 472–478.
Vogelsang-O'Dwyer, M., Petersen, I. L., Joehnke, M. S., Sørensen, J. C., Bez, J., Detzel, A., et al. (2020). Comparison of Faba bean protein ingredients produced using dry fractionation and isoelectric precipitation: Techno-functional, nutritional and environmental performance. *Foods, 9*(3), 322.
Voutsinas, L. P., Cheung, E., & Nakai, S. (1983). Relationships of hydrophobicity to emulsifying properties of heat denatured proteins. *Journal of Food Science, 48*(1), 26–32.
Wang, X., Cheng, L., Wang, H., & Yang, Z. (2022). Limited Alcalase hydrolysis improves the thermally-induced gelation of quinoa protein isolate (QPI) dispersions. *Current Research in Food Science, 5*, 2061–2069.
Wang, Z., Li, Y., Jiang, L., Qi, B., & Zhou, L. (2014). Relationship between secondary structure and surface hydrophobicity of soybean protein isolate subjected to heat treatment. *Journal of Chemistry, 2014*.
Wei, Z., & Huang, Q. (2020). Impact of covalent or non-covalent bound epigallocatechin-3-gallate (EGCG) on assembly, physicochemical characteristics and digestion of ovotransferrin fibrils. *Food Hydrocolloids, 98*, Article 105314.
Wittek, P., Walther, G., Karbstein, H. P., & Emin, M. A. (2021). Comparison of the rheological properties of plant proteins from various sources for extrusion applications. *Foods, 10*(8), 1700.
Wood, K., Mata, J. P., Garvey, C. J., Wu, C.-M., Hamilton, W. A., Abbeywick, P., et al. (2018). QUOKKA, the pinhole small-angle neutron scattering instrument at the OPAL research reactor, Australia: Design, performance, operation and scientific highlights. *Journal of Applied Crystallography, 51*(2), 294–314.
Wynnychuk, C., Jo, Y.-J., Chu, Y., & Chen, L. (2021). Long-term stable emulsions prepared from lentil protein fibrillar aggregates. *Food Structure, 29*, Article 100204.
Xia, W., Siu, W. K., & Sagis, L. M. (2021). Linear and non-linear rheology of heat-set soy protein gels: Effects of selective proteolysis of β-conglycinin and glycinin. *Food Hydrocolloids, 120*, Article 106962.
Xu, W., Sun, H., Jia, Y., Jia, Y., Ning, Y., Wang, Y., et al. (2023). Pickering emulsions synergistic stabilized with konjac glucomannan and xanthan gum/lysozyme nanoparticles: Structure, protection and gastrointestinal digestion. *Carbohydrate Polymers, 305*, Article 120507.
Yang, Z., de Campo, L., Gilbert, E. P., Knott, R., Cheng, L., Storer, B., et al. (2022). Effect of NaCl and CaCl2 concentration on the rheological and structural characteristics of thermally-induced quinoa protein gels. *Food Hydrocolloids, 124*, Article 107350.
Yang, Z., Hemar, Y., Hilliou, L., Gilbert, E. P., McGillivray, D. J., Williams, M. A., et al. (2016). Nonlinear behavior of gelatin networks reveals a hierarchical structure. *Biomacromolecules, 17*(2), 590–600.
Yang, J. T., Wu, C. S. C., & Martinez, H. M. (1986). Calculation of protein conformation from circular dichroism. *Methods in Enzymology, 130*, 208–269. Elsevier.
Yang, Z., Yang, H., & Yang, H. (2018). Effects of sucrose addition on the rheology and microstructure of κ-carrageenan gel. *Food Hydrocolloids, 75*, 164–173.

Yildiz, G., Andrade, J., Engeseth, N. E., & Feng, H. (2017). Functionalizing soy protein nano-aggregates with pH-shifting and mano-thermo-sonication. *Journal of Colloid and Interface Science, 505*, 836–846.

Zhang, R., Luo, L., Yang, Z., Ashokkumar, M., & Hemar, Y. (2021). Formation by high power ultrasound of aggregated emulsions stabilised with milk protein concentrate (MPC70). *Ultrasonics Sonochemistry, 81*, Article 105852.

Zhang, S., Holmes, M., Ettelaie, R., & Sarkar, A. (2020). Pea protein microgel particles as Pickering stabilisers of oil-in-water emulsions: Responsiveness to pH and ionic strength. *Food Hydrocolloids, 102*, Article 105583.

Zhang, R., Cheng, L., Luo, L., Hemar, Y., & Yang, Z. (2021). Formation and characterisation of high-internal-phase emulsions stabilised by high-pressure homogenised quinoa protein isolate. *Colloids and Surfaces A: Physicochemical and Engineering Aspects, 631*, Article 127688.

Zhang, Y., Lu, Y., Zhang, R., Gao, Y., & Mao, L. (2021). Novel high internal phase emulsions with gelled oil phase: Preparation, characterization and stability evaluation. *Food Hydrocolloids, 121*, Article 106995.

Zhao, M., Xiong, W., Chen, B., Zhu, J., & Wang, L. (2020). Enhancing the solubility and foam ability of rice glutelin by heat treatment at pH12: Insight into protein structure. *Food Hydrocolloids, 103*, Article 105626.

Zhong, Z., & Xiong, Y. L. (2020). Thermosonication-induced structural changes and solution properties of mung bean protein. *Ultrasonics Sonochemistry, 62*, Article 104908.

Zhu, L., Li, Y., Yu, J., Liu, H., Li, H., Liu, X., et al. (2023). Interfacial behavior and emulsifying property of thermosonication-treated soy glycinin. *LWT, 187*, Article 115368.

Zou, Y., Yang, X., & Scholten, E. (2018). Rheological behavior of emulsion gels stabilized by zein/tannic acid complex particles. *Food Hydrocolloids, 77*, 363–371.